The challenge of identifying *INTEGRAL* sources on the Galactic plane

Raffaella Landi[a], Loredana Bassani[a], Gabriele Bruni[b], Manuela Molina[c], Nicola Masetti[a,d], Angela Malizia[a], Mariateresa Fiocchi[b], Angela Bazzano[b], Pietro Ubertini[b]

[a]*INAF – Osservatorio di Astrofisica e Scienza dello Spazio, Via Piero Gobetti 93/3, Bologna, 40129, Italy,*
[b]*INAF – Istituto di Astrofisica e Planetologia Spaziali, Via del Fosso del Cavaliere 100, Roma, 00133, Italy,*
[c]*INAF – Istituto di Astrofisica Spaziale e Fisica Cosmica, Via Alfonso Corti 12, Milano, 20133, Italy,*
[d]*Instituto de Astrofísica, Facultad de Ciencias Exactas, Universidad Andrés Bello, Fernández Concha 700, Las Condes, Santiago RM, Chile,*

Abstract

The International Gamma-ray Astrophysics Laboratory (*INTEGRAL*) has been surveying the sky above 20 keV since its launch in 2002 providing new insights into the nature of the sources that populate our Universe at soft γ-ray energies. The latest IBIS/ISGRI survey lists 929 hard X-ray sources, of which 113 are reported as unidentified, i.e. lacking a lower energy counterpart or simply not studied in other wavebands. To overcome this lack of information, we either browsed the X-ray archives, or, if no data in the X-ray band were available, we requested Target of Opportunity (ToO) observations with the X-ray Telescope (XRT) on-board the Neil Gehrels *Swift* Observatory. Following this approach, we selected a sample of 10 objects for which X-ray data were key to investigate their nature. We found a single X-ray association for all of the sources, except for IGR J16267−3303, for which two X-ray detections were spotted within the IBIS positional uncertainty. We then browsed multi-waveband archives to search for counterparts to these X-ray detections at other wavelengths and analysed X-ray spectral properties to determine their nature and association with the high-energy emitter. As a result of our analysis, we identified the most likely counterpart for 7 sources, although in some cases its nature/class could not be definitely assessed on the basis of the information collected. Interestingly, SWIFT J2221.6+5952, first reported in the 105-month *Swift*/Burst Alert Telescope (BAT) survey, is the only source of the sample for which we did not find any counterpart at radio/optical/IR wavebands. Finally, we found that two IBIS source, IGR J17449−3037 and IGR J17596−2315 are positionally associated with a *Fermi* Large Area Telescope (LAT) object.

Keywords: catalogues, surveys, gamma rays: observations, X-ray: general

1. Introduction

In the last decade, high-energy instruments with imaging capabilities like *INTEGRAL*/IBIS (Ubertini et al., 2003) and *Swift*/BAT (Barthelmy et al., 2005) have revolutionised our view of the 20–100 keV sky by providing the deepest surveys of the entire celestial sphere. Overall, around 2000 sources have been discovered so far, a large part of which were new detections, either persistent or transient and their number is continuously increasing due to the constant accumulation of exposure. Many of these high-energy emitters have been optically identified thanks to X-ray follow-up observations that allow one to pinpoint, within the much smaller positional uncertainty, a single (rarely a double) optical/infrared (IR) counterpart, which is then classified through optical spectroscopy (see, e.g., Koss et al. 2017, Karasev et al. 2018, Butler et al. 2009, Masetti et al. 2010, Masetti et al. 2012, Masetti et al. 2013). Despite this large effort from the astronomical community over the years, a significant sample of sources are still unidentified/unclassified mainly due to their location on the Galactic plane, where identification and classification procedures are much more difficult. This is mainly due to the Galactic plane being more optically/IR crowded and also more reddened than the extragalactic sky. Crowdedness makes the identification of a single/double optical/IR counterpart difficult, as many objects may fall within the few arcseconds accuracy of the X-ray localisation, while reddening makes optical and often IR follow-up observations more challenging. Variability is another issue since objects seen occasionally by high-energy instruments may not be bright enough during follow-up at lower energies. For these reasons, a multi-wavelength approach, coupled to the most stringent positional accuracy available, is the key to deal with unidentified/unclassified IBIS and BAT

Email addresses: raffaella.landi@inaf.it (Raffaella Landi), loredana.bassani@inaf.it (Loredana Bassani), gabriele.bruni@inaf.it (Gabriele Bruni), manuela.molina@inaf.it (Manuela Molina), nicola.masetti@inaf.it (Nicola Masetti), angela.malizia@inaf.it (Angela Malizia), mariateresa.fiocchi@inaf.it (Mariateresa Fiocchi), angela.bazzano@inaf.it (Angela Bazzano), pietro.ubertini@inaf.it (Pietro Ubertini)

sources lying along the Galactic plane. Sometimes, however, even this procedure is not sufficient to pinpoint a single counterpart and/or to understand the source nature/class, making the identification of these objects even more challenging.

Bearing this in mind, we focused our attention on those sources, listed in the latest IBIS/ISGRI survey (Krivonos et al., 2022), which are located on the Galactic plane and are still unidentified. Firstly, our approach was to browse X-ray archives in search of data at lower energies that can help in identifying the X-ray and hence the optical/IR counterpart; furthermore, information in the X-ray band allows the characterisation of these sources in terms of spectral shape, flux, absorption properties and variability. This approach allowed us to single out a set of 10 high-energy sources located at $|b| \lesssim 10^{\circ}$. For three of them (IGR J16267−3303, IGR J18006−3426, and IGR J19193+0754), we also applied for XRT ToO observations, which were executed. The aim of these requests was to obtain on-source observations which were not available in the archives.

We then made use of lower energy X-ray observations (*Swift*/XRT, *XMM-Newton*, and *Chandra*) to provide the best available position, some variability information and X-ray spectral parameters. The best position of the optical/IR counterpart, thus pinpointed, was then searched on available catalogues to provide insights into the source nature and a tentative classification. As a result, we were able to spot the likely counterpart for 7 out of 10 objects; in the case of IGR J17327−4405, IGR J18006−3426, and IGR J19193+0754 the enhanced X-ray positional uncertainties are still too large to pinpoint a unique optical/IR association. Intriguingly, SWIFT J2221.6+5952 is the only source of the sample for which we did not find any counterpart at any other wavelength investigated; with this respect, being the source located in a crowded region of the Galactic plane, we encourage further multi-band follow-up observation to shed light on the nature of this high-energy emitter.

As a by-product of this analysis, we found that 4 *INTEGRAL* objects are close to an unclassified *Fermi*/LAT source and that two of them (IGR J17449−3037 and IGR J17596−2315) have probably GeV associations.

The paper is structured as follows: in Sect. 2 we briefly present the method adopted for the *Swift*/XRT and *XMM-Newton* data reduction and the criteria assumed for the spectral analysis. Sect. 3 is devoted to the discussion of the results for each source of our sample, making use of multi-frequency information. Conclusions are drawn in Sect. 4.

2. Data reduction and analysis

To characterise the behaviour of the selected sample in X-rays, we used data acquired with the X-ray Telescope (XRT, 0.3–10 keV, Burrows et al. 2005) on board the Neil Gehrels *Swift* Observatory and with the *XMM-Newton* satellite. The details of the observations are reported in the Appendix A (see Table A.1).

To produce XRT screened event file we made use of the standard data pipeline package (XRTPIPELINE v. 0.13.7). All data were extracted only in the Photon Counting (PC) mode (Hill et al., 2004). Source events were extracted within a circular region with a radius of 20 pixels (1 pixel corresponding to 2.36 arcseconds) centred on the source position, while background events were extracted from a source-free region nearby the X-ray source of interest. To search for X-ray detections both within the 90% and 99% IBIS error circles, we analysed, by means of XIMAGE v. 4.5.1, the 0.3–10 keV image of each observation and, then, estimated the X-ray position using the task XRTCENTROID v. 0.2.9. In most cases we smoothed the X-ray images to visualise better the X-ray counterparts; the presence of grains/features inside the XRT field of view (FoV) are indisputably spurious.

The source spectra were then extracted from the corresponding event file using the XSELECT v. 2.5a software and generally binned using GRPPHA in an appropriate way, so that the χ^2 statistic could be applied. For sources with fewer counts (typically around 50–60), data were binned to have at least 5 count per energy bin and the Cash statistic (Cash, 1979) was adopted.

We used version v. 014 of the response matrices and created the individual ancillary response file using the task XRTMKARF v. 0.6.4.

Data from the European Photo Imaging Cameras (EPIC-pn, 0.1–12 keV, Turner et al. 2001) were reprocessed using the *XMM-Newton* Standard Analysis Software (SAS) version 20.0.0 and employing the latest available calibration files. Only patterns corresponding to single and double events (PATTERN<4) were taken into account and the standard selection filter FLAG = 0 was applied. EPIC-pn nominal exposures were filtered for periods of high background, resulting in the cleaned exposures reported in Table A.1. Source counts were extracted from a circular region of typically 20–30 arcseconds radius centred on the source (depending on the source brightness), while background spectra were extracted from two circular regions of 20 arcseconds radius each in source-free areas. The ancillary response matrices (ARF) and the detector response matrices (RMF) were generated using the XMM-SAS tasks ARFGEN and RMFGEN and spectral channels were rebinned in order to achieve a minimum of 20 counts per bin. For EPIC observations we also adopted the same approach as for XRT to search for likely counterparts.

Table 1 lists all of the 10 IBIS sources analysed here together with their position and significance in σ units as listed in Krivonos et al. (2022); following Krivonos et al. (2007), we have used a 4.2 and 3.0 arcminutes search radius at 90% confidence level (c.l.) for a source detected at 5–6σ and around 10σ c.l., respectively. For each of these γ–ray emitters, we then report the position and relative uncertainties (at 90% c.l.) of the likely counterpart/s

detected by XRT and *XMM-Newton* within the 90% and 99% IBIS error circles, as well as the count rate in the 0.3–10 keV and 3–10 keV energy bands, and their angular distance from the *INTEGRAL* position. The X-ray counterparts highlighted in the XRT and *XMM-Newton* images are labelled as reported in Table 1.

The spectral analysis was performed by means of the XSPEC package (v. 12.12.1, Arnaud 1996); errors are quoted at 90% c.l. for one parameter of interest ($\Delta\chi^2 = 2.71$).

For objects with more than one pointing, we analysed each single observation and discussed the presence of source variability in each dedicated section. When the quality of the data was not good enough to perform a reliable spectral analysis, to improve the signal-to-noise ratio, we summed together all the available observations and analysed the average spectra. In the first instance, we adopted, as our basic model, a simple power law passing through Galactic absorption (Kalberla et al., 2005). If this baseline model was not sufficient to fit the data, we then introduced extra spectral components as required. The results of this analysis are shown in Table 2 and Table 3 where we report the best-fit parameters obtained by fitting XRT and *XMM-Newton* data, respectively. A more detailed description of the X-ray spectral analysis results is given in a dedicated section for each source.

3. Notes on individual sources

In the following, we present results on each individual source in the X-ray, optical, IR, and radio (see Table B.1 in the Appendix B) band, discussing the overall properties found for each candidate counterpart.

3.1. IGR J16173−5023

IGR J16173−5023 was first analysed by Tomsick et al. (2012), who used a *Chandra* observation performed on October 11, 2011 to search for the X-ray counterpart of this high-energy emitter. They found two possible associations: a brighter one with a 2–10 keV flux of 5.87×10^{-12} erg cm^{-2} s^{-1} and a dimmer one with a 2–10 keV flux of 0.5×10^{-12} erg cm^{-2} s^{-1}. No clear optical/IR counterpart could be found for the brighter source, but the detection of an iron line at 6.8 keV suggested the possibility that this might be a Cataclysmic Variable (CV) in the Norma region.

We analyse here XRT observations performed in 2012, 2017 and 2019 (see Table A.1). The X-ray data indicate the presence of a single source inside the IBIS 90% positional uncertainty (see Figure 1), which is detected at $\sim12\sigma$ c.l. over the 0.3–10 keV energy range (see Table 1). The source average spectrum is well fitted with the basic model (photon index of ∼1.5 and a 2–10 keV flux of $\sim3\times10^{-12}$ erg cm^{-2} s^{-1}) plus thermal emission (Raymond-Smith model in XSPEC, Raymond and Smith 1977) to account for the excess below 2 keV (see Table 2).

The source location and associated positional uncertainty indicate that this is the brightest source seen by

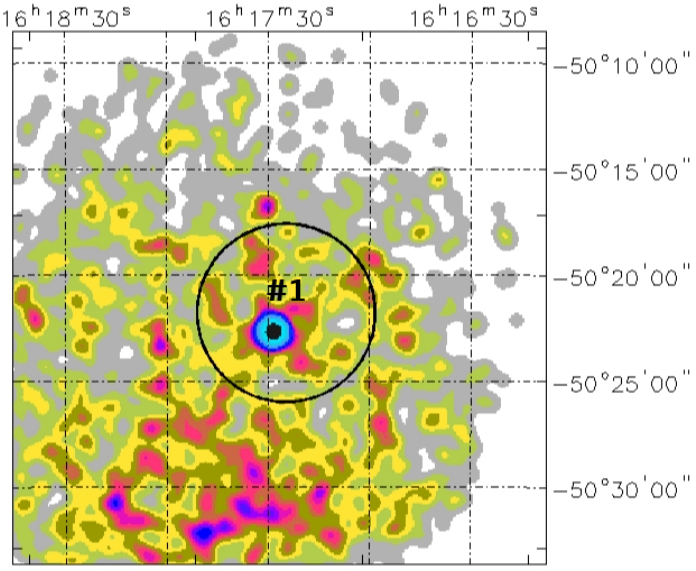

Figure 1: XRT 0.3–10 keV image of the region surrounding IGR J16173−5023. The only XRT detection lies within the 90% IBIS positional uncertainty (black circle).

Chandra and further suggest that this is likely the counterpart to the persistent *INTEGRAL* object. The XRT pointings also indicate that, although persistent, this is also a variable emitter since the X-ray flux increased by a factor of 4 during XRT monitoring (from 2012 to 2019).

Using the *Chandra* position (from Tomsick et al. 2012) and a more restrictive positional uncertainty (R.A.(J2000) = $16^h17^m28^s.26$, Dec.(J2000) = $-50°22'42''.50$, error radius of 1 arcsecond) with respect the XRT one, it is possible to pinpoint a single optical/IR counterpart designated as source 5935091920522976256 in the *Gaia* DR3 catalogue (Gaia Collaboration et al., 2021); the latest release of the catalogue (*Gaia* DR3 Part 1 Main source, 2022[1] and originally in Gaia Collaboration et al. 2021) provides the following apparent magnitudes: G = 18.09, BP = 18.64, RP = 17.36, and an absolute parallax of 0.494 ± 0.140. Inferring the distance from *Gaia* parallax is not a trivial issue nor is it easy to evaluate reddening corrections for *Gaia* magnitudes; for these reasons, we rely on the parameters provided by the same *Gaia* DR3 catalogue (version 2022) which quote a source distance of 1630 pc, an absolute G magnitude of 6.15 and a reddening corrected $BP - RP$ colour of 0.79. We further notice that the source is considered variable in *Gaia* magnitude with a typical amplitude of 0.14 mag in G, RP, and 0.2 mag in BP (Mowlavi et al., 2021).

Using this information and referring to the study of Gaia Collaboration et al. (2019) on variable stars, it is possible to locate the source in the colour-absolute magnitude diagram close to the region populated by CV, making IGR J16173−5023 a CV candidate as first suggested by Tomsick et al. (2012). Going more in detail, we also compared

[1]available at http://vizier.nao.ac.jp/viz-bin/Cat?I/355.

the source location in the *Gaia* colour-absolute magnitude diagram of Abril et al. (2020) with that of various types of CV, finding that it might be an Intermediate Polar (IP) of around 7-hour period. This is fully compatible with the detection of an iron line at 6.8 keV seen by *Chandra* (Tomsick et al., 2012), as well as with the source detection by IBIS, being IPs one of the most likely hard X-ray emitters seen by *INTEGRAL* (Lutovinov et al., 2020; Landi et al., 2009). Moreover, based on the 17–60 keV flux reported by Krivonos et al. (2022) and the luminosity function of hard X-ray emitting CVs (Suleimanov et al., 2022), the luminosity of IGR J16173−5023 at 1.6 kpc turns out to be 1.6×10^{33} erg s^{-1}, which further strenghtens the IP classification.

We also notice that the source is an Hα emitter with magnitude 17.17±0.01 as inferred from the VST Photometric Hα Survey of the Southern Galactic Plane and Bulge (VPHAS+, Drew et al. 2014); the source is also present in the VISTA Variables in the Via Lactea Survey (VVV, Minniti et al. 2017) with IR magnitudes $J = 16.052 \pm 0.011$, $H = 15.708 \pm 0.022$, and $Ks = 15.164 \pm 0.030$.

We conclude that the source is a Galactic object at a distance of 1.6 kpc and very likely a CV of the IP type.

3.2. IGR J16267−3303

IGR J16267−3303 is a new *INTEGRAL* source, listed for the first time in the Krivonos et al. (2022) catalogue. No X-ray observations had been available until we requested a *Swift*/XRT ToO observation performed on January 20, 2023 (see Table A.1). The source is interesting because of its proximity to a *Fermi* object (4FGL J1627.4−3301), which was associated with a *ROSAT* Faint source (1RXS J162725.1−330322[2]) and tentatively classified as a blazar of uncertain type (Fan et al., 2022, and references therein). Figure 2 shows the XRT image of the sky region of interest with overlapping the IBIS and LAT positional uncertainties and the location of the *ROSAT* source. Thanks to the positional accuracy of XRT, the position of the *ROSAT* Faint object can be determined with a greater precision, namely at R.A.(J2000) = $16^h27^m26^s.80$, Dec.(J2000) = $-33°02'00''.90$, with an associated uncertainty of 6 arcseconds. Unfortunately, this is still too large to identify a single optical/IR counterpart. We also note that, despite the low statistical quality of the data do not allow a full analysis, the *ROSAT* source could be extended in X-rays. However, this object lies outside the IBIS error circle, which leads us to exclude an association between the IBIS and *Fermi* sources, although their positional uncertainties overlap slightly; we then focus, in the following, our attention only to the IBIS counterpart.

The XRT image indicates the presence of two X-ray detections inside the 90% IBIS positional uncertainty (see zoomed section in Figure 2 and also Table 1): source #1 is

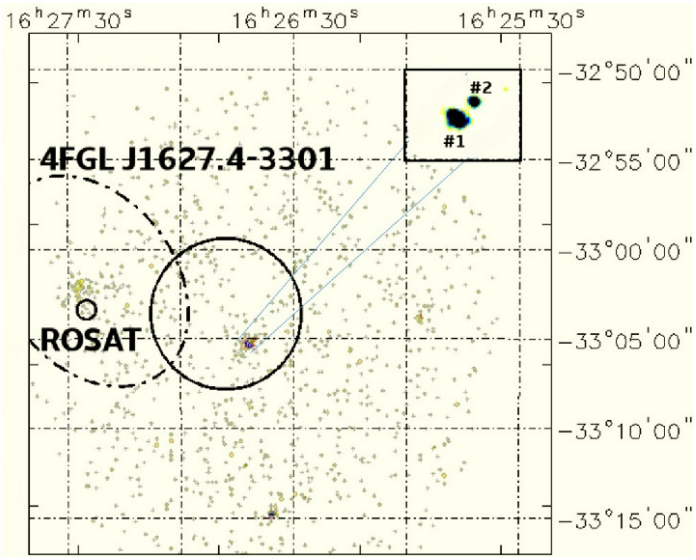

Figure 2: XRT 0.3–10 keV image of the region surrounding IGR J16267−3303. Two X-ray sources (see close-up inset of the region) lie within the 90% IBIS positional uncertainty (black circle). Also plotted are the error ellipse of the *Fermi* source 4FGL J1627.4−3301 (black dash-dotted ellipse), which partially intersects the IBIS error circle, and the *ROSAT* Faint source 1RXS J162725.1−330322 displayed with its positional uncertainty (smaller black circle).

the brightest and also hardest of the two and, therefore, the most likely counterpart. The X-ray average spectrum is of poor statistical quality to allow a full characterisation of the source behaviour, but our basic model provides either a flat spectrum ($\Gamma \sim -0.7$) and a 2–10 keV flux of $\sim 5 \times 10^{-12}$ erg cm^{-2} s^{-1} or an absorbed spectrum ($N_{\rm H(intr)} \sim 4 \times 10^{22}$ cm^{-2}) if a photon index of 1.8 is assumed (see Table 2).

Figure 3 depicts the optical image, from the Dark Energy Camera Plane Survey 2 (DECaPS, Saydjari et al. 2023), of the region surrounding source #1. Within the XRT error circle we find two objects (sources A and B in the Figure) which belong to the *Gaia* DR3 catalogue (version 2022, originally in Gaia Collaboration et al. 2021). Source A, which is the closest source to the XRT best position (R.A.(J2000) = $16^h26^m42^s.1351$, Dec.(J2000) = $-33°05'19''.937$), is dim ($G = 21.00 \pm 0.03$) and difficult to classify. Source B (R.A.(J2000) = $16^h26^m42^s.2762$, Dec.(J2000) = $-33°05'22''.117$) is further apart but, on the basis of its properties, easier to categorise as an active galaxy viewed through the Galactic plane: it is extended (see Figure 3) and its *WISE* (Wide-field Infrared Survey Explorer all sky survey, Wright et al. 2010) colours are typical of an AGN ($W1-W2 = 0.81$, $W2-W3 = 2.7$, $W3-W4 = 2.45$). Using these 3 colours and the 3-dimensional *WISE* colour space diagram discussed by D'Abrusco et al. (2019) (see their Figure 6) it is possible to characterise further the source as a blazar of the BL Lac type. The lack of radio emission in the source at 1 mJy level (see Table B.1) is surprising but not unexpected (Massaro et al., 2017).

Source #2 is dimmer (by a factor of 14) in X-rays and softer than object #1, but it is still a possible extra as-

[2]This source is located at: R.A.(J2000) = $16^h27^m25^s.10$, Dec.(J2000) = $-33°03'22''.50$, error radius of 32 arcseconds.

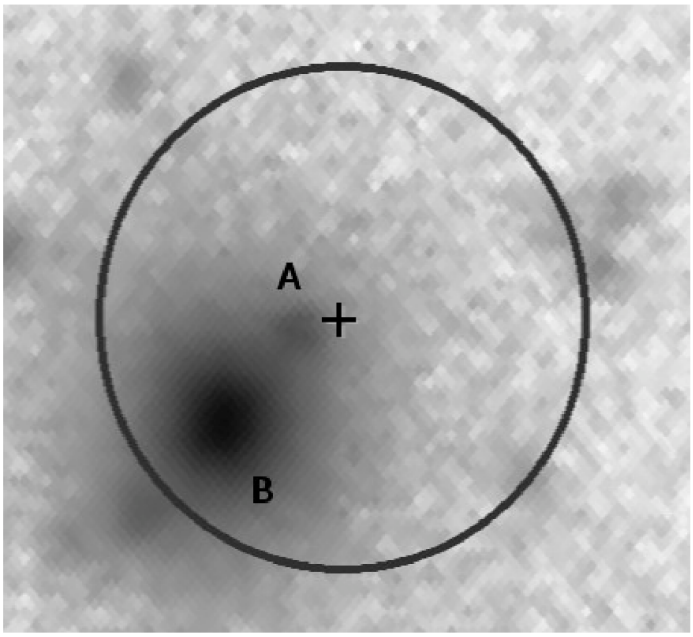

Figure 3: DECaPS image of the region in the field of IGR J16267−3303 and centred around source #1 located at R.A.(J2000)= $16^h26^m42^s.05$ and Dec.(J2000) = $-33°05'19''.66$. Within the XRT positional uncertainty (black circle, 6 arcsecond in radius) are clearly visible the two *Gaia* sources labelled with A and B (see text).

sociation. Its average spectrum provides a 2–10 keV flux of $\sim 2 \times 10^{-13}$ erg cm^{-2} s^{-1} by assuming the basic model with the photon index frozen to 1.8. Within the XRT positional uncertainty we find only one source which is also listed in the *WISE* catalogue with colours once more typical of an AGN, and possibly of a BL Lac type blazar ($W1 - W2 = 0.62$, $W2 - W3 = 2.38$, $W2 - W3 \geq 3.27$, D'Abrusco et al. 2019).

Also this possible counterpart is not detected in radio at a flux limit of 1 mJy (see Table B.1), thus making the *WISE* colours the only signature of its AGN nature.

Based on the available information we suggest that source #1 is the most likely counterparts to IGR J16267−3303, although a contribution from source #2 is possible; in any case, this *INTEGRAL* emitter is most likely an extragalactic source viewed through the Galactic plane.

3.3. IGR J17315−3221

This *INTEGRAL* source was recently discussed by Ferrigno et al. (2022) (see their Appendix). Although previously classified in the literature as a possible supergiant X-ray binary, these authors suggested that it may be the product of a data analysis artifact and thus should be disregarded for future studies. They motivated this conclusion with the lack, within 2 arcminutes from the IBIS position reported by Krivonos et al. (2012), of an X-ray counterpart in the XRT image obtained by summing observations made over the period 2012–2016. They also reanalysed all *INTEGRAL* archival data available around the position of IGR J17315−3221 and found no detection at the source position. We note, however, that: a) the 2.2 arcminutes error radius provided by (Krivonos et al., 2012) is only at the 68% c.l. and b) that the source is further confirmed in the most recent catalogue of Krivonos et al. (2022).

We therefore reanalysed *Swift*/XRT and *XMM-Newton* observations of the source to search for an X-ray counterpart to this high-energy emitter within the 90% of the position uncertainty associated with the most recent *INTEGRAL* location. First, we analysed individual XRT pointings (performed on September 1, 2012 and during the period August 8–20, 2016, see Table A.1) to search for source variability. The lack of evidence for a significant flux variation led us to add all observations together to improve the signal-to-noise ratio and pinpoint the most likely counterpart. In Figure 4, we show the XRT image, in the 0.3–10 keV energy band, of the region surrounding IGR J17315−3221, where it is evident the presence of a source at the border of the 90% *IBIS* error circle. The source position and relative error are listed in Table 1. The average XRT spectrum, modelled with our basic model, provides a flat photon index ($\Gamma \sim 0.7$) and a 2–10 keV flux of $\sim 2 \times 10^{-12}$ erg cm^{-2} s^{-1} (see Table 2).

Then, we browsed the *Chandra* Source Catalogue 2.1[3], finding that the XRT source was present (2CXO J173113.7−322204, detected at $\sim 7\sigma$ c.l.), albeit slightly dimmer (by a factor around 1.8). The best *Chandra* position is at R.A.(J2000) = $17^h31^m13^s.68$, Dec.(J2000) = $-32°22'04''.80$ (error radius of 0.76 arcseconds), while the 0.5–7 keV flux is $(7.10 \pm 1.00) \times 10^{-13}$ erg cm^{-2} s^{-1}.

We also turned our attention to the *XMM-Newton* data, as we find that a pointing was recently performed towards this region on September 14, 2022 (see Table A.1). The analysis of the *XMM-Newton* data provides a further detection of the source at a position compatible with that of XRT and *Chandra*. This observation, moreover, yields the best yet available X-ray spectrum of the source. Our basic model applied to the *XMM-Newton* data shows residuals hinting at an excess around 6 keV. The addition of an iron line component, with the line width σ fixed to 0.01 keV, is required only at 93% ($\Delta\chi^2/\nu = 6/2$), yielding a line centroid $E_C \sim 6.4$ keV and an Equivalent Width (EW) around 208 eV; the 0.2–12 keV flux is $\sim 1.9 \times 10^{-12}$ erg cm^{-2} s^{-1} (see Table 3).

Moreover, we note that the source is reported also as an *XMM-Newton* Slew Survey (Saxton et al., 2008) detection with a 0.2–12 keV flux of $(1.7 \pm 0.6) \times 10^{-12}$ erg cm^{-2} s^{-1} in a slew made on August 29, 2014. Since the source was monitored by various X-ray detectors over a quite large period of years, we can infer a flux variability by a factor up to 1.8 from 2016 to 2022.

Thanks to the restricted source location obtained by *Chandra*, we are also able to pinpoint a possible optical/IR counterpart to the source, even if it is located in

[3]available at: https://asc.harvard.edu/csc/about2.1.html.

Table 1: *INTEGRAL*/IBIS position and source detection significance of the 10 selected sources. For each high-energy emitter, the objects detected by XRT or *XMM-Newton*, within the 90% IBIS positional uncertainties, are reported along with their relative count rates in the 0.3–10 and 3–10 keV energy range, and their angular distance from the *INTEGRAL* position. The XRT and *XMM-Newton* error radii are given at 90% confidence level.

XRT source	R.A. (J2000)	Dec. (J2000)	error (arcsecond)	Count rate (0.3–10 keV) (10^{-3} counts s^{-1})	Count rate (3–10 keV) (10^{-3} counts s^{-1})	Distance[a] (arcmin)	Instr.
IGR J16173−5023 (R.A.(J2000) = $16^h17^m24^s.72$**, Dec.(J2000)** = $-50°21'46''.80$, 7.4σ)							
#1	$16^h17^m28^s.37$	$-50°22'40''.22$	3.84	41.18 ± 3.30 (12.5σ)	20.54 ± 2.30 (8.9σ)	0.70	XRT
IGR J16267−3303 (R.A.(J2000) = $16^h26^m48^s.00$**, Dec.(J2000)** = $-33°03'36''.00$, 4.4σ)							
#1	$16^h26^m42^s.05$	$-33°05'19''.66$	6.00	26.77 ± 3.50 (7.6σ)	20.37 ± 3.00 (6.8σ)	2.42	XRT
#2	$16^h26^m40^s.41$	$-33°05'00''.22.$	6.00	9.11 ± 2.00 (4.6σ)	3.91 ± 1.30 (3.0σ)	2.35	XRT
IGR J17315−3221 (R.A.(J2000) = $17^h31^m33^s.60$**, Dec.(J2000)** = $-32°21'36''.00$, 4.2σ)							
#1	$17^h31^m13^s.85$	$-32°22'05''.26$	3.88	21.20 ± 2.10 (10.1σ)	13.32 ± 1.70 (7.8σ)	4.19	XRT
IGR J17327−4405 (R.A.(J2000) = $17^h32^m45^s.60$**, Dec.(J2000)** = $-44°06'00''.00$, 7.3σ)							
#1	$17^h32^m53^s.05$	$-44°07'29''.40$	3.66	47.52 ± 2.70 (17.6σ)	32.07 ± 2.20 (14.6σ)	1.72	XRT
IGR J17449−3037 (R.A.(J2000) = $17^h44^m55^s.20$**, Dec.(J2000)** = $-30°37'12''.00$, 5.3σ)							
#1	$17^h45^m07^s.97$	$-30°39'05''.90$	1.1	53.38 ± 3.22 (16.6σ)	47.95 ± 2.99 (16.0σ)	3.58	XMM
IGR J17596−2315 (R.A.(J2000) = $17^h59^m38^s.40$**, Dec.(J2000)** = $-23°16'12''.00$, 9.4σ)							
#1	$17^h59^m46^s.56$	$-23°13'56''.43$	4.32	8.24 ± 2.60 (3.2σ)	5.28 ± 1.90 (2.8σ)	3.62	XRT
IGR J18006−3426 (R.A.(J2000) = $18^h00^m40^s.80$**, Dec.(J2000)** = $-34°27'00''.00$, 5.0σ)							
#1	$18^h00^m50^s.55$	$-34°23'20''.58$	4.10	27.31 ± 3.80 (7.2σ)	5.94 ± 1.80 (3.3σ)	3.66	XRT
IGR J19071+0716 (R.A.(J2000) = $19^h07^m07^s.20$**, Dec.(J2000)** = $+07°16'12''.00$, 4.2σ)							
#1	$19^h07^m06^s.33$	$+07°20'04''.58$	5.02	5.03 ± 1.00 (5.0σ)	2.84 ± 0.77 (3.7σ)	4.15	XRT
IGR J19193+0754 (R.A.(J2000) = $19^h19^m16^s.80$**, Dec.(J2000)** = $+07°54'28''.80$, 4.7σ)							
#1	$19^h19^m06^s.57$	$+07°59'28''.48$	6.21	13.52 ± 3.50 (3.9σ)	–	5.25	XRT
SWIFT J2221.6+5952 (R.A.(J2000) = $22^h22^m09^s.60$**, Dec.(J2000)** = $+59°52'48''.00$, 5.2σ)							
#1	$22^h21^m59^s.82$	$+59°51'52''.33$	4.10	18.07 ± 2.10 (8.6σ)	8.82 ± 1.50 (5.9σ)	1.81	XRT

[a]: Angular distance from the *INTEGRAL* position.

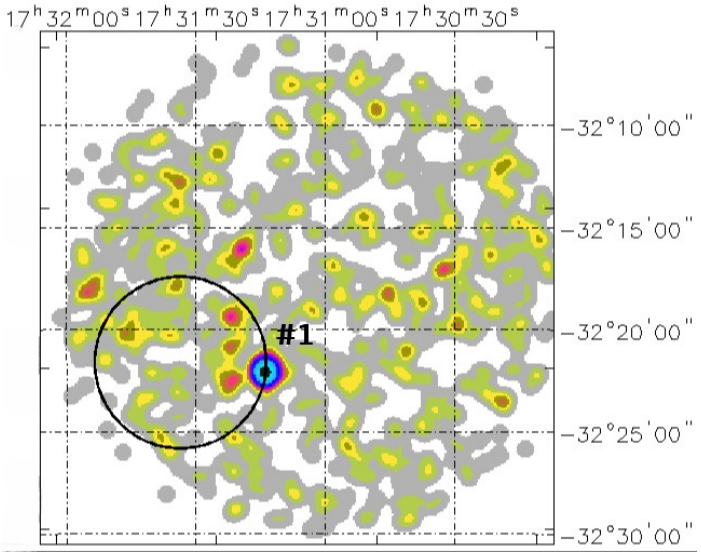

Figure 4: XRT 0.3–10 keV image of the region surrounding IGR J17315−3221. XRT detects only one source located at the border of the 90% IBIS positional uncertainty (black circle).

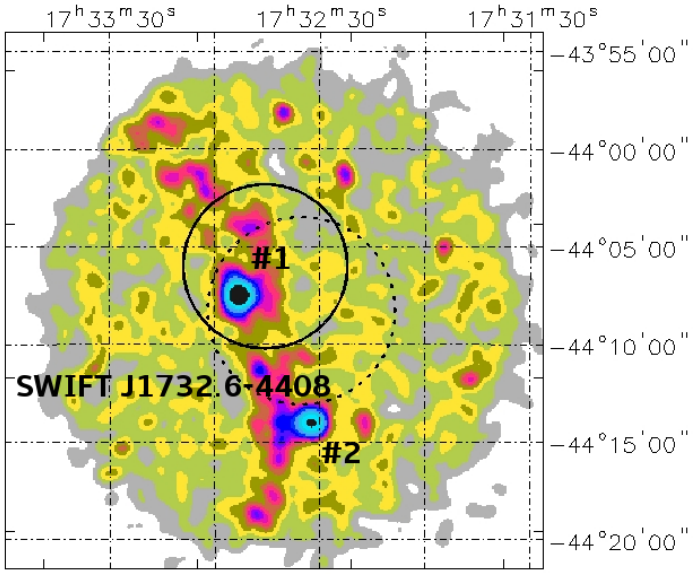

Figure 5: XRT 0.3–10 keV image of the region surrounding IGR J17327−4405. XRT detects a source within the 90% IBIS error circle (black circle), which also lies inside the positional uncertainty (black-dotted circle) of the *Swift*/BAT source SWIFT J1732.6−4408. Source #2 is a transient object detected in the February 24, 2019 pointing (see text).

a crowded region of the Galactic plane (Scorpius region). Within the *Chandra* positional uncertainty there is one single object reported in the *Gaia* DR3 catalogue as source 4054812795194499968 (Gaia Collaboration et al., 2021); it has an apparent G magnitude of 20.68 ± 0.01 and a $BP-RP$ colour index of 1.90. Its distance can be found in the catalogue of Bailer-Jones et al. (2018) with a value of $4.33^{+2.14}_{-2.19}$ kpc. Adopting this distance, we obtain an absolute G magnitude of 7.5 (unfortunately we could not find a reliable reddening correction for this source); using this and the $BP-RP$ colour of 1.90, we locate the source in the *Gaia* colour-absolute magnitude diagram close to the binary sequence zone (Gaia Collaboration et al., 2019). The *Gaia* object is also present in the VPHAS+ catalogue (Drew et al., 2014) with an Hα magnitude of 20.59 ± 0.13.

However, at near-IR frequencies the situation is more complex as the VVV catalogue (Minniti et al., 2017) reports two possible counterparts: the *Gaia* object (VVV J173113.69−322204.99) and another source (VVV J173113.64−322205.28) nearby, so for the time being we cannot pinpoint the actual optical/IR counterpart for this source.

We suggest in any case that this is likely a variable Galactic source, possibly of binary nature.

3.4. IGR J17327−4405/SWIFT J1732.6−4408

This source is also reported in recent *Swift*/BAT catalogues (see for example the 105- and the 157-month surveys[4], Oh et al. 2018), where it is listed as a source of unknown class and with no X-ray counterpart. However, this sky region was observed by XRT on a number of occasions over the 2017–2021 period, although most of these pointings are of low exposure (see Table A.1). The 0.3–10 keV image of the region surrounding IGR J17327−4405, obtained stacking together all the XRT pointings, is displayed in Figure 5: two sources are clearly detected, although only one falls within the positional uncertainty of both IBIS and BAT. Since the statistics on individual pointing is quite poor and the flux variation not so large (by a factor around 1.2), we decided to sum all the observations together and perform the spectral analysis of the average data.

The spectrum of source #1, well described by our basic model, shows a flat spectral index ($\Gamma \sim 0$), and requires an additional thermal component (MEKAL in XSPEC; Mewe et al. 1985) with a $kT \sim 0.14$ keV; the 2–10 keV flux is $\sim 6.7 \times 10^{-12}$ erg cm^{-2} s^{-1} (see Table 2).

Unfortunately, the XRT positional uncertainty, even if small, is insufficient to pinpoint a unique optical candidate. For example, in the *Gaia* DR3 catalogue (version 2022) (Gaia Collaboration et al., 2021) there are three objects within the X-ray positional uncertainty, all of which are likely Galactic with distances in the range 2–6 kpc; one of these is also variable in *Gaia*, suggesting a possible association with the XRT source. This ambiguity can only be resolved by means of a *Chandra* pointing, which should be able to pinpoint a unique association.

The other source (#2 in Figure 5), is also an interesting object as it is extremely variable: it was quite bright on February 27, 2019 reaching a flux of $\sim 1.7 \times 10^{-11}$ erg cm^{-2} s^{-1}. However, the source was barely detected on February 1, 2019 with a 2–10 keV flux $\sim 1.4 \times 10^{-12}$ erg cm^{-2} s^{-1}; no detection was found in the previous and following

[4] available at: https://swift.gsfc.nasa.gov/results/bs157mon/

pointings.

The source is located at R.A.(J2000) = $17^h32^m32^s.55$, Dec.(J2000) = $-44°14'02''.10$, with an associated error of 3.8 arcseconds. It is detected at $\sim 16\sigma$ and $\sim 7\sigma$ c.l. in the 0.3–10 keV energy range and above 3 keV, respectively. Our basic model (power law with $\Gamma = 1.30^{+0.58}_{-0.77}$) does not provide a good fit to the data as the residuals support the presence of an excess below 2 keV that can be modelled with a thermal bremsstrahlung with $kT = 0.30^{+0.20}_{-0.13}$ keV.

Given the extremely variable behaviour of this object versus the persistent nature of the hard X-ray source #1, as well as its location outside the positional uncertainty of both IBIS and BAT, we exclude any association between this and source #2, but note that this XRT source is nevertheless an interesting discovery for its extremely variable behaviour.

We therefore conclude that source #1 is the likely association and further suggests it is a Galactic source.

3.5. IGR J17449−3037

Also IGR J17449−3037 is a new *INTEGRAL* detection (Krivonos et al., 2022), close to the Galactic centre region. The source is particularly interesting since it lies in a region populated by GeV/TeV sources; in particular, the IBIS error circle crosses the positional uncertainty of the *Fermi* source 2FHL J1745.1−3035 (see the *XMM-Newton* view of the sky region around IGR J17449−3027 shown in Figure 6) reported in the catalogue of Ackermann et al. (2016), which lists objects detected above 50 GeV. Given the overlap of the two positional errors and the detection of a single X-ray source within both, we assume that the IBIS and LAT objects are associated and that the *XMM-Newton* detection is their low-energy counterpart.

This hard *Fermi* source is itself spatially coincident with the extended source HESS J1745−303, which may contain up to three different sources (Aharonian et al., 2008); indeed, the position of 2FHL J1745.1−3035 is compatible with TeV emission region C (the second brightest region in the complex, see Figure 1 in Aharonian et al. 2008). However, the nature of the source is probably more complex because 2FHL J1745.1−3035 is slightly brighter at 1 TeV than the entire H.E.S.S. region and has also a harder spectrum[5] (spectral index of 1.25±0.38 estimated by *Fermi* versus 2.17 ± 0.11 as measured by H.E.S.S.). Besides, the situation is complicated by emission at lower GeV energies and by the vicinity of the Galactic centre. For these reasons, we only consider valid the association between IGR J17449−3037 and 2FHL J1745.1−3035 for the remainder of the discussion. Although the source had been monitored by XRT on various occasions (see Table A.1), it was never detected, thus implying a flux level below 2×10^{-13} erg cm^{-2} s^{-1} over the 0.2–12 keV waveband. When all these observations are summed together a marginal detection at

[5]2FHL J1745.14−3035 is one of the 3 hardest sources in the 2FHL catalogue, implying a high-energy SED peak in the TeV band.

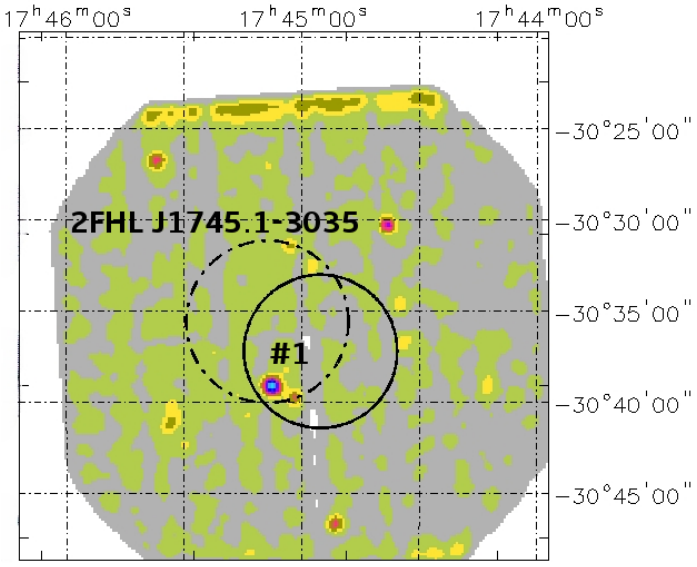

Figure 6: *XMM-Newton* pn 0.2–12 keV image of the region surrounding IGR J17449−3037. There is only one source within both the black circle and the black-dashed-dotted error ellipse, which represent the positional uncertainty of IGR J17449−3037 and 2FHL J1745.1−3035, respectively.

2.4σ is obtained: the source position is at R.A.(J2000) = $17^h45^m07^s.20$, Dec.(J2000) = $-30°39'02''.30$ (error radius of 6 arcseconds); the average source flux results to be 1.8×10^{-13} erg cm^{-2} s^{-1} in the 0.2–12 keV band, confirming the lack of detection in single XRT snapshots performed over the period 2012–2021. Fortunately, this sky region was also monitored by *XMM-Newton* and, luckily, the source was detected over at least 4 occasions: 3 times during individual pointings on March 21, 2001, on April 3, 2017, and on March 16, 2021 (see Table A.1) and one time during a slew of the satellite performed on March 9, 2014. Archival data indicate a change in flux during *XMM-Newton* monitoring that we investigated by analysing the source behaviour during each snapshot. As shown in Table 3, the X-ray spectrum, with respect to the basic model, requires extra absorption and is characterised by a flat photon index. The source was detected at a 0.2–12 keV flux level of $(1.73 \pm 0.22) \times 10^{-12}$, $(1.35 \pm 0.08) \times 10^{-12}$, and $(1.49 \pm 0.09) \times 10^{-12}$ erg cm^{-2} s^{-1} during the individual pointing (see Table 3).

If we also take into account the 0.2–12 keV flux estimate of $(0.73 \pm 0.39) \times 10^{-12}$ erg cm^{-2} s^{-1} obtained during *XMM-Newton* slew, we assess a source variability by a factor of 2.4 between individual *XMM-Newton* observations and by a factor of ∼10 comparing to XRT pointings. We also note that these changes can occur on short time scale, as evident from a comparison between the 2021 *XMM-Newton* and XRT measurements (by a factor of over 10 over less than a month time scale). *XMM-Newton* also allows a better positioning of the source as reported in Table 1, with an accuracy at 1-arcsecond level.

Due to the *XMM-Newton* reduced positional uncer-

Table 2: Data analysis results of the averaged *Swift*/XRT spectra. Frozen parameters are written in square brackets; errors are given at the 90% confidence level.

Source	$N_{\rm H(Gal)}$ (10^{22} cm^{-2})	$N_{\rm H(int)}$ (10^{22} cm^{-2})	kT (keV)	Γ	$\chi^2/d.o.f.$	$C-stat/d.o.f.$	$F_{(2-10\ \rm keV)}$ (10^{-12} erg cm^{-2} s^{-1})
IGR J16173−5023							
#1[a]	2.13	–	$0.19^{+0.32}_{-0.11}$	$1.51^{+0.53}_{-0.59}$	6.1/11	–	3.48 ± 0.24
IGR J16267−3303							
#1	0.158	–	–	$-0.61^{+0.41}_{-0.51}$	–	9.7/10	4.71 ± 0.61
	0.158	$3.79^{+2.59}_{-1.23}$	–	[1.8]	–		2.14 ± 0.27
#2	0.158	–	–	[1.8]	–	4.2/3	0.18 ± 0.05
IGR J17315−3221							
#1	1.24	–	–	$0.67^{+0.36}_{-0.40}$	15.7/10	–	2.18 ± 0.18
IGR J17327−4405							
#1[b]	0.307	–	0.14 ± 0.08	-0.04 ± 0.16	11.2/20	–	6.72 ± 0.32
IGR J17596−2315							
#1	1.23	–	–	[1.8]	–	5.5/7	0.86 ± 0.17
IGR J18006−3426							
#1	0.228	–	–	$1.13^{+0.43}_{-0.46}$	6.5/7	–	3.11 ± 0.34
IGR J19071+0716							
#1	1.56	–	–	$1.46^{+0.88}_{-0.96}$	–	5.7/5	0.35 ± 0.07
IGR J19193+0754							
#1[b]	0.554	–	$0.60^{+0.52}_{-0.31}$	–	–	2.9/2	0.018 ± 0.04
SWIFT J2221.6+5952							
#1	0.828	–	–	$0.90^{+0.44}_{-0.47}$	5.6/8	–	1.33 ± 0.15
	0.828	$0.81^{+0.81}_{-0.53}$	–	[1.8]	8.2/8	–	0.89 ± 0.10

[a]: In this case, the best-fit model requires a thermal component (Raymond-Smith model in XSPEC);

[b]: For this source, the best fit model requires a thermal component (MEKAL in XSPEC).

Table 3: *XMM-Newton* spectral analysis results; errors are given at the 90% confidence level.

Source	$N_{H(Gal)}$ (10^{22} cm^{-2})	$N_{H(int)}$ (10^{22} cm^{-2})	Γ	$\chi^2/d.o.f.$	$F_{(0.2-12\ keV)}$ (10^{-12} erg cm^{-2} s^{-1})
IGR J17315−3221					
#1[a]	1.24	–	1.08 ± 0.09	95.8/88	1.95 ± 0.05
IGR J17449−3037					
obs1					
#1	0.968	$9.39^{+6.88}_{-7.02}$	$1.25^{+2.09}_{-1.48}$	12.4/12	1.73 ± 0.22
obs2					
#1	0.968	$7.56^{+4.59}_{-3.26}$	$0.93^{+0.73}_{-0.62}$	21.0/21	1.35 ± 0.08
obs3					
#1	0.968	$3.01^{+2.30}_{-1.76}$	$0.19^{+0.51}_{-0.47}$	19.5/23	1.49 ± 0.09
IGR J17596−2315					
#1	1.23	–	$0.15^{+0.43}_{-0.49}$	9.1/6	1.52 ± 0.15

[a]: For this source the best-fit model includes a narrow Gaussian line: energy centroid $E_c = 6.36 \pm 0.07$ keV and $EW = 208^{+120}_{-116}$ eV.

tainty, we are also able to find a unique counterpart in the VIRAC (VVV Infrared Astrometric Catalogue, Smith et al. 2018) source 195465789 located at R.A.(J2000) = $17^h45^m08^s.0180$, Dec.(J2000) = $-30°39'04''.993$, having Ks magnitude of 16.707 ± 0.031 and a total proper motion of 199.88 ± 81.14 mas/yr. Hence, we have a source that emits from few keV to GeV energies, it is variable in X-rays, quite hard in GeV, and must be of Galactic nature since the VIRAC source has a proper motion. We also note that hard sources in the 2FHL catalogue (with $\Gamma < 2$) tend to be associated with Galactic objects, thus confirming that we are dealing with a close-by source and also with an efficient particle accelerator. Among Galactic sources that emit above 50 GeV, many are Supernovae remnants (SNRs), Pulsar Wind Nebulae (PWNs) and PWN/SNRs complexes with a small contribution (only 5 objects) of binary systems (Ackermann et al., 2016). SNRs tend to have softer spectra and are generally not variable in X-rays, while strong variability can be a distinctive properties of binary systems and less of PWNs. Also we note that no radio emission is detected in the direction of the source, which is unlikely for a SNR or even a PWN. Thus, we conclude that this may be a new GeV (maybe TeV) emitter possibly associated with a binary system or, at a lower level, a PWN.

Unfortunately, the location of the source close to the Galactic plane does not favour optical or IR observations (although we note that the VIRAC source is quite bright in Ks magnitude), but *Chandra* high-resolution data could allow one to confirm or exclude a PWN association by finding whether extended X-ray emission is observed or not.

3.6. IGR J17596−2315

This new source, reported by Krivonos et al. (2022), is located in the Sagittarius region. It is another case where a *Fermi* source, 4FGL J1759.5−2312, lies nearby. This GeV source is still unclassified and poorly studied: its emission can be described by a power law with a photon index of 2.4 ± 0.1 and a 0.1–100 GeV flux of 2.1×10^{-11} erg cm^{-2} s^{-1} (Abdollahi et al., 2022). The only association reported is with a radio source belonging to the NRAO VLA Sky Survey (NVSS, Condon et al. 1998), namely NVSS J175948−230944, of unknown type.

The 0.3–10 keV XRT image of the region surrounding IGR J17596−2315, displayed in Figure 7, shows the presence of an X-ray source located at the border of the 90% IBIS error circle that also lies within the positional uncertainty of the *Fermi* source 4FGL J1759.5−2312; interestingly, this X-ray source is not associated with the radio

source NVSS J175948−230944, suggested as possible counterpart to the *Fermi* emitter. Moreover, the XRT image indicates the presence of diffuse emission around the source of interest here, which is probably part of the SNR W28 located to the south and is large enough to extend up to the region pointed by XRT. Despite the presence of this emission, the overlapping of IBIS and LAT positional uncertainties, as well as the presence of a relatively bright XRT source inside both, points to a likely association between the 3 emitters.

Checking individual XRT pointings, we found that the XRT source was visible only on two occasions (at around 2.8σ), namely on February and August 2014 and undetected in other occasions (probably due to the low exposure times of the pointings). Unfortunately, because of the low statistical quality of the X-ray data, we could not characterise the source emission in each epoch. Therefore, we summed together the data and perform the spectral analysis of the average spectrum. By fitting the data with our basic model and fixing the photon index to 1.8, we found a 2–10 keV flux of $\sim 8.6 \times 10^{-13}$ erg cm^{-2} s^{-1} (see also Table 2).

The source was also observed by *XMM-Newton* on March 19–20, 2003; since we did not find evidence for flux variability in the data, we stack together the observations and performed the analysis of the average spectrum. Our basic model yields a good fit to the data (see Table 3), providing a flat photon index ($\Gamma \sim 0.2$) and a 0.2–12 keV flux of $\sim 1.5 \times 10^{-12}$ erg cm^{-2} s^{-1}. We then applied the *XMM-Newton* best-fit model to the XRT data, finding that in a similar energy band the flux is comparable ($\sim 1.2 \times 10^{-12}$ erg cm^{-2} s^{-1}), thus suggesting no flux variation for over a decade. The *XMM-Newton* data are also useful to restrict the positional uncertainty of the source, which reduces to 2 arcseconds for R.A.(J2000) = $17^{\rm h}59^{\rm m}46^{\rm s}.495$, Dec.(J2000) = $-23°13'58''.39$.

The *XMM-Newton* data confirm the presence of diffuse emission suggested by XRT and raise the possibility that we are looking at a bright X-ray spot in the outskirts of the SNR W28.

Within the *XMM-Newton* error circle we find the VIRAC (Smith et al., 2018) source 223122211, which is characterised by a proper motion of 1.24 ± 0.53 mas/yr and IR magnitudes $J = 15.919 \pm 0.016$, $H = 14.363 \pm 0.014$ and $Ks = 13.561 \pm 0.015$. The source is also visible in the Panoramic Survey Telescope & Rapid Response System (Pan-STARRS) catalogue (Chambers et al., 2016), with an I magnitude of 21.43 ± 0.16; finally, it is also reported in the VPHAS survey (Drew et al., 2014) with a photometric Hα magnitude of 20.76 ± 0.13. The observation of proper motion clearly points to a Galactic object, most likely a star of some type (with a probability $\geq 90\%$, according to the UKIDSS-DR6 Galactic Plane Survey, Lucas et al. 2008). On the other hand, the near-IR data allow us to estimate the index $Q = (J - H) - 1.7(H - K)$, which provides a way to separate early-type from late-type stars (Reig and Milonaki, 2016). While the latter are mostly

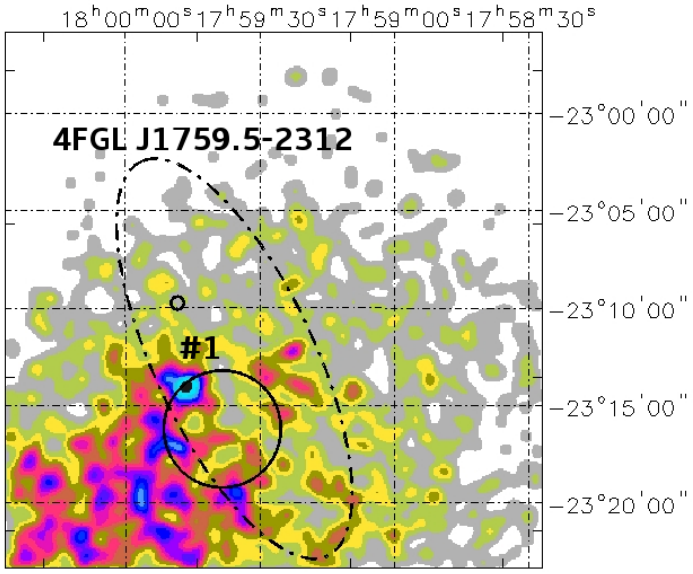

Figure 7: XRT 0.3–10 keV image of the region surrounding IGR J17596−2315. The only XRT detection lies at the border of the 90% IBIS positional uncertainty (black circle) and is located within the error ellipse of 4FGL J1759.5−2312 (black-dashed-dotted ellipse). The smaller black circle depicts the position of the radio source NVSS J175948−230944, suggested to be the counterpart to the *Fermi* object.

concentrated around values of $Q = 0.4 - 0.5$ (which correspond to spectral types K to M), the early-type objects typically display $Q < 0$ (Reig and Milonaki, 2016). In this case, $Q = 0.17 \pm 0.03$ suggests an early-type object.

No radio emission is detected from this X-ray source (see Table B.1), which is however located at the outskirt of the SNR W28 and close to a radio filament as clearly visible in the Rapid ASKAP Continuum Survey (RACS, Lacy et al. 2020) image of the region (see Figure 8); unfortunately, it is difficult with present data to assess whether the source is part of the remnant structure or simply an X-ray emitting object behind it.

The bright radio source located north of the IBIS source is NVSS J175948−230944, suggested to be the counterpart to the *Fermi* source 4FGL J1759.5−2312. In reality, NVSS did not pinpoint the correct position of the source, better localised in the catalogues of compact radio sources in the Galactic plane by White et al. (2005), where it is listed with a 1.4 and 5 GHz flux of 53.6 ± 0.2 and 157.5 ± 2.5 mJy, respectively. The source is also visible in images by RACS (Lacy et al., 2020), with a 0.88 GHz flux of 330 ± 21 mJy and by the Very Large Array Sky Survey (VLASS, McConnell et al. 2020), with a 3 GHz flux of 118 ± 12 mJy. The RACS position position is at R.A.(J2000) = $17^{\rm h}59^{\rm m}47^{\rm s}.77$, Dec.(J2000) = $-23°10'41''.75$ (2.5 arcseconds uncertainty); the morphology is that of a complex source showing a bright core with extended emission on one side as evident from the VLASS image shown in Figure 9. The source is pretty weak in optical with a Pan-STARRS I magnitude of 21.36 ± 0.09 and relatively bright in IR with UKIDSS-DR6

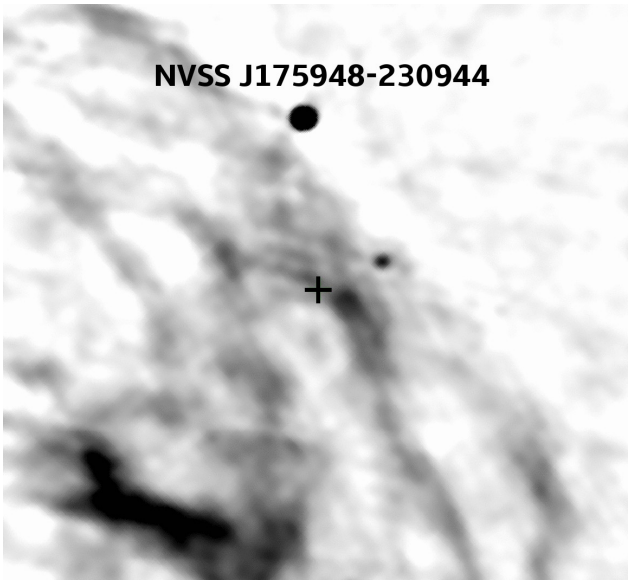

Figure 8: RACS radio image of the region surrounding IGR J17596−2315. The black cross depicts the position of the source detected in X-rays, which is located at R.A.(J2000) = $17^h59^m46^s.56$ and Dec.(J2000) = −23°13′56″.43. Also highlighted is the radio source NVSS J175948−230944 that was proposed as the counterpart to the *Fermi* source 4FGL J1759.5−2312.

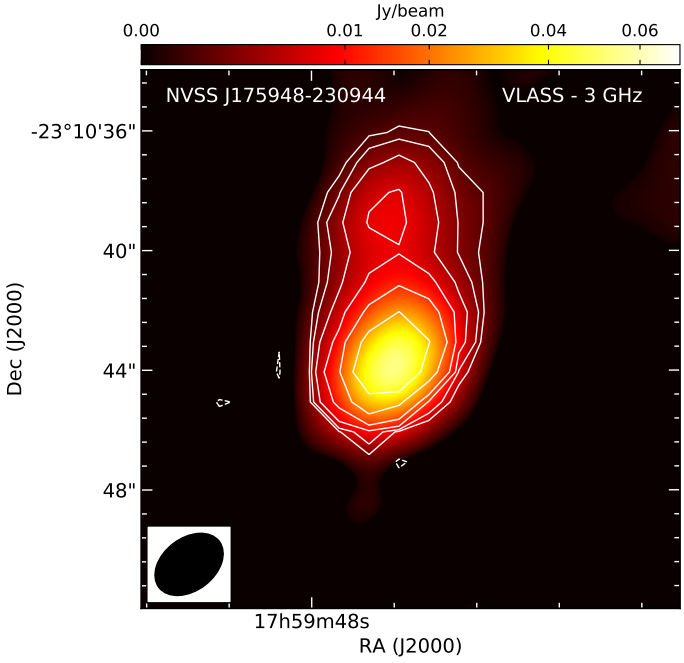

Figure 9: VLASS image of NVSS J175948−230944.

J and H magnitudes of 15.455 ± 0.006 and 13.975 ± 0.04, respectively. This source could be a blazar seen behind our Galaxy and thus be a possible counterpart to the *Fermi* object. On the other hand, the presence of an X-ray source with emission up to 100 keV indicates that the association with 4FGL J1759.5−2312 is very likely.

3.7. IGR J18006−3426

Also IGR J18006−3426 is a new addition to the *INTEGRAL* list of high-energy emitters by Krivonos et al. (2022), who associated the source with the XRT catalogued object 2SXPS J180050.6−342322 (error radius of 4.9 arcseconds, see Evans et al. 2020) discovered thanks to a previous pointing performed on February, 2013; however, the reported 0.3–10 keV flux was quite high (1.6×10^{-11} erg cm^{-2} s^{-1}) for a source seen at only few sigma c.l., as typically observed with XRT. Reanalysing these data we found the source to be barely detected (3.5σ c.l. overall) at the border of the field of view (roughly 12 arcminutes from the pointing) and only in one of the two observations (that on February 8, 2013); its observed flux, estimating by fitting the data with our basic model, was also well below the reported one (around 4.6×10^{-12} erg cm^{-2} s^{-1} in the 0.3–10 keV energy range), thus casting some doubts on its real presence and/or true X-ray properties.

For these reasons, we triggered a *Swift*/XRT ToO observation at the position of the IBIS source, which was performed on February 6, 2023 (see Table A.1). The source detection is confirmed at the location reported in Table 1, with a 0.3–10 keV flux of $\sim 3 \times 10^{-12}$ erg cm^{-2} s^{-1} evaluated adopting our basic model, which is slightly below our 2013 estimate. However, given the large uncertainties, we assume that the source did not vary over this long time span and therefore summed the two pointings together to enhance the signal-to-noise-ratio. The resulting image is shown in Figure 10, where the unique X-ray counterpart is visible within the IBIS positional uncertainty of 4.2 arcminutes. The average spectrum is well described by the basic model and it is characterised by a flat spectrum ($\Gamma \sim 1.1$) (see Table 2).

Despite the XRT positional uncertainty being too large to pinpoint a unique optical/IR counterpart, we note that a radio source, VLASS1QLCIR J180050.84−342322.0 is detected by VLASS (McConnell et al., 2020) within the soft X-ray error circle; its flux is 2.37±0.26 mJy at 3 GHz and its morphology is reported as compact (in reality, it is slightly resolved at the resolution of the instrument with a deconvolved size of $2.32 \pm 0.59 \times 0.52 \pm 0.44$ arcseconds). The source is also reported in the NVSS survey (Condon et al., 1998), with a 1.4 GHz flux of 2.9 ± 0.6 mJy, while in RACS (Lacy et al., 2020) it is detected with a 0.88 GHz flux of 7.85 ± 0.3 mJy (see Table B.1). While a comparison between VLASS and NVSS fluxes suggests a flat spectral index ($\alpha = -0.29$), that between RACS and VLASS/NVSS indicates instead an unphysical steep α value (from –0.96 up to –2.14); this probably hints at a change in flux at lower frequencies over a time span of around 30 years.

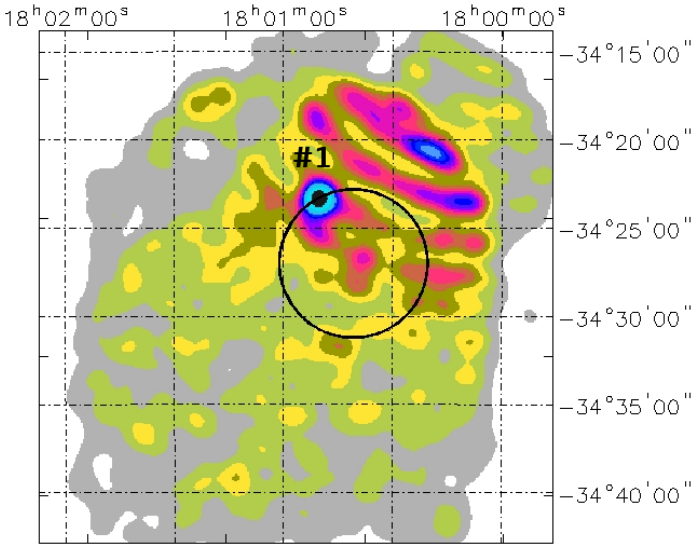

Figure 10: XRT 0.3–10 keV image of the region surrounding IGR J18006–3426. The only X-ray detection is located at the border of the 90% IBIS positional uncertainty (black circle).

This source is also listed in the *AllWISE* catalogue (Cutri et al., 2021) with magnitudes $W1 = 13.386 \pm 0.085$, $W2 = 12.186 \pm 0.038$, $W3 = 8.960 \pm 0.035$ and $W4 = 6.358 \pm 0.072$; the source IR colours are therefore $W1 - W2 = 1.2$ and $W2 - W3 = 3.23$, which are typical of highly efficiently accreting AGN (Secrest et al., 2015). Using a third colour $W3 - W4 = 2.6$ and the three-dimensional *WISE* colour space discussed by D'Abrusco et al. (2019) (see their Figure 6) it is possible to characterise further the source as a blazar and more specifically as a Flat Spectrum Radio Quasar (FSRQ); this is confirmed by the listing of the source in the *Gaia* large amplitude variables (Mowlavi et al., 2021) and VIVACE (VIrac VAriable Classification Ensemble, Molnar et al. 2022) catalogues as a long-period variable. The slightly extended structure seen in VLASS could also suggests a core plus jet morphology. We thus conclude that the radio source is a blazar behind the Galactic plane.

Taking into account that a chance coincidence cannot be excluded in this crowded region and that other objects are present within the XRT positional uncertainty, we consider the association between the IBIS emitter and the VLASS source quite probable but not definitive until a more accurate X-ray position is provided. If this association is confirmed, then IGR J18006−3426 can be classified as a new blazar shining behind our Galaxy.

3.8. IGR J19071+0716

This source, first reported in the Krivonos et al. (2017) list of *INTEGRAL* sources and located in the Aquila region, is still unidentified in the latest catalogue by the same authors (Krivonos et al., 2022), where it is highlighted as a low signal-to-noise source (<4.5σ c.l.). This may be due to the weak or variable nature of the source. Indeed, this sky region was observed several times by XRT (albeit with different exposures, see Table A.1), but only in 2010 during a long pointing, and marginally in 2012, a single source was detected inside the IBIS error circle (see Figure 11). These observations allow us to locate the source with higher precision and to restrict significantly the IBIS positional uncertainty (see Table 1). Unfortunately, due to the low signal-to-noise ratio of the X-ray data, we could perform a reliable spectral analysis only for the longest pointing. The source spectrum can be approximated by a flat power law ($\Gamma \sim 1.5$) with a 2–10 keV flux of $\sim 3.5 \times 10^{-13}$ erg cm^{-2} s^{-1} (see Table 2). However, from the observation performed in 2012 we can only infer a 2–10 keV flux around 3.4×10^{-13} erg cm^{-2} s^{-1}, if we assume our basic model with photon index frozen to 1.8, thus indicating that the source did not change in flux from 2010 to 2012.

Despite the good positional uncertainty of the XRT data, the location of the source on the Galactic plane prevents us from pinpointing one single optical/IR counterpart. Fortunately, this sky region was also observed by *Chandra* on February 18, 2018: a source (2CXO J190706.3+072001 detected at 4.1σ c.l.), compatible with the XRT one, is found at R.A.(J2000) = $19^{\rm h}07^{\rm m}06^{\rm s}.24$, Dec.(J2000) = $+07°20'01''.90$ (error radius of 1.8 arcseconds), while the 0.5–7 flux is $(5.5 \pm 1.7) \times 10^{-14}$ erg cm^{-2} s^{-1}.

The source was also detected during 4 *XMM-Newton* measurements performed during different periods of time (on October 15, 2003, on April 23–25, 2004 and, most recently, on October 22, 2018; Webb et al. 2020); over this period the 0.2–12 keV source flux changed from $(1 - 1.3) \times 10^{-12}$ erg cm^{-2} s^{-1} (2003–2004) to 0.45×10^{-12} erg cm^{-2} s^{-1} (2018); this last source state is similar to that observed by XRT on November 2010 and February 2012. Thus, the source flux decreased significantly (roughly by a factor > 2) over a few years time scale.

Within the *Chandra* positional uncertainty, we find only one IR object listed in the UKIDSS-DR6 Galactic Plane Survey (Lucas et al., 2008) as UGPS J190706.32+072001.8, with magnitudes $J = 18.809 \pm 0.088$, $H = 18.132 \pm 0.117$, and $K = 17.415 \pm 0.129$. The index $Q = (J-H) - 1.7(H-K) = -0.54 \pm 0.23$, estimated from the near-IR data, points to an early-type star if the source is Galactic (Reig and Milonaki, 2016).

Lacking other information, the nature of this counterpart remains elusive, although follow-up observations are now feasible thanks to the reduced X-ray positional uncertainty and the presence of an IR source within it.

We finally note that an unidentified *Fermi* source, 4FGL J1906.9+0712/3FHL J1907.0+0713, lies close-by and intersects the IBIS error circle in its southern part (see Figure 11). This *Fermi* emitter is an interesting source because of a detected break in the γ-ray spectrum at around 130 MeV and a change in spectral slope to a value around 3 (Abdollahi et al., 2022), which is a strong indication that the *Fermi* source is a cosmic ray accelerator; however, its properties are not typical of a SNR, a confirmed

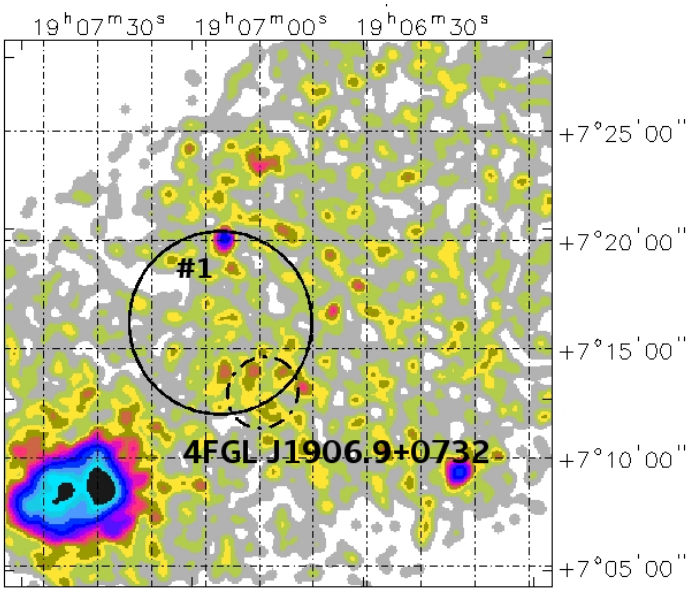

Figure 11: XRT 0.3–10 keV image of the region surrounding IGR J19071+0716. The XRT detection lies at the border of the IBIS error circle (black circle). Also plotted is the positional uncertainty of the *Fermi* source 4FGL J1906.9+0712 (black-dashed-dotted ellipse), which partially intersects the IBIS error circle.

type of cosmic accelerator. Massive protostar outflows, stellar winds from runaway stars, colliding wind binaries, and young stellar clusters have also been considered as candidate sources (Ergin et al., 2021).

Unfortunately, the only X-ray source detected within the IBIS positional uncertainty is outside the *Fermi* error ellipse, thus casting doubts on the possible association between the two high-energy emitters.

3.9. IGR J19193+0754

This *INTEGRAL* source is most likely associated with 1RXS J191907.6+075921, a *ROSAT* Bright source (0.1–2.4 keV flux of 1.5×10^{-12} erg cm^{-2} s^{-1}) located at a distance of 5.4 arcminutes and with a positional error of 13 arcseconds. As demonstrated by Stephen et al. (2006), such an association is nearly secure and sometimes sufficient to restrict the X-ray source positional uncertainty, but in this case not enough to pinpoint a unique optical counterpart.

Despite this, 1RXS J191907.6+075921 was associated in the literature with TYC 1042−2233−1/ASAS J191907+0759.3, a rotating variable star (Haakonsen and Rutledge, 2009; Kiraga, 2012) with an average V magnitude of 11.4 and a period of 3.16 days[6]. According to the All Sky Automated Survey (ASAS, Pojmanski 2002), the source is very close to us (around 300 parsec) and was classified as a Rotational Variable, i.e. a star that changes in its apparent brightness due to large spots on its surface. These stars are subdivided into several types like Ap stars, some Am stars, RS CVn stars, and BY Dra stars, most of which are generally not found to be strong emitters in the 20–100 keV.

Due to these uncertainties (relatively large soft X-ray error circle and unlikely X-ray emission from the proposed counterpart), we have requested a ToO observation of the source with *Swift*/XRT, which was performed, on February 20, 2023 (see Table A.1). The XRT image of the sky region is shown in Figure 12, where two sources are detected inside (source #1) and in proximity (source #2) of the 99% IBIS error circle. However, only source #1 is of the right intensity to be a likely counterpart to the *INTEGRAL* detection (see coordinates in Table 1). The source location confirms that this is the *ROSAT* Bright object but, unfortunately, the XRT exposure was not long enough to restrict considerably the positional uncertainty, which resulted to be only half the previous one in radius. The best-fit model is described only by a thermal component (MEKAL in XSPEC), with a temperature around 0.6 keV. The 0.1–2.4 flux is $\sim 1.4 \times 10^{-14}$ erg cm^{-2} s^{-1}, thus indicating a variability by a factor of 100 if compared to the *ROSAT* value.

The XRT error circle is still too large to pinpoint a single counterpart: for example *Gaia* DR3 (Gaia Collaboration et al., 2021) lists 6 objects, 5 of which are however extremely weak in optical, but one is quite bright. This is indeed the star associated in the literature with the *ROSAT* detection, which is also reported as variable in various catalogues. The source is listed in the *Gaia* DR3 catalogue (version 2022) with an apparent G magnitude of 10.87, a colour index $BP - RP = 1.46$, and a distance of 325.9 pc; we also note that in *Gaia* it was classified as a RS Canum Venaticorum type of variable star, again with a period of 3.16 days (see Gaia Collaboration, 2022)[7].

The *Gaia* DR3 catalogue also quotes the source reddening corrected absolute G magnitude and colour index ($M\_G = 2.6$ and 1.1, respectively); these values are compatibles with those expected for RS Canum Venaticorum variable stars (see Gaia Collaboration et al. 2019).

This type of stars is not typically found in the *INTEGRAL* catalogue; a few of such objects were classified through optical spectroscopy (Masetti et al., 2008, 2012, 2013), while GT Mus (Bird et al., 2016; Sguera et al., 2016) was discovered thanks to bright outbursts observed over the observing period (see also Sasaki et al. 2021). If this association is confirmed, this would be another such system caught by *INTEGRAL*.

Therefore, if the association is correct, then the source must have been caught by XRT during a period of low flux, while presumably the *INTEGRAL* detection could be related to one or more outburst events. Otherwise, this is not the correct association and a more refined positional error, such as one provided by *Chandra*, is needed to pinpoint the right lower-energy counterpart.

[6] see https://asas-sn.osu.edu/variables/abac3e8b-492d-51a7-8a8e-be996938828b for more information.

[7] available at: https://vizier.cds.unistra.fr/viz-bin/VizieR?-source=I/354.

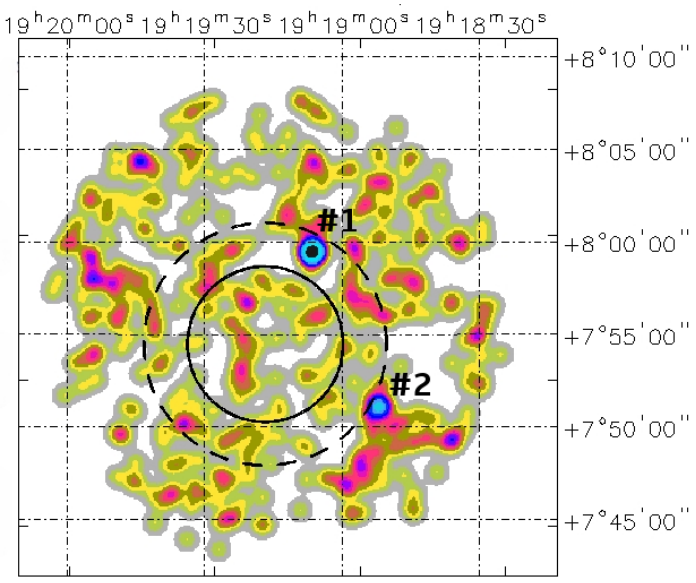

Figure 12: XRT 0.3–10 keV image of the region surrounding IGR J19193+0754. The XRT detection, described in the text and labelled as source #1, is outside the 90% but inside the 99% IBIS positional uncertainty (continuous and dashed black circles), respectively.

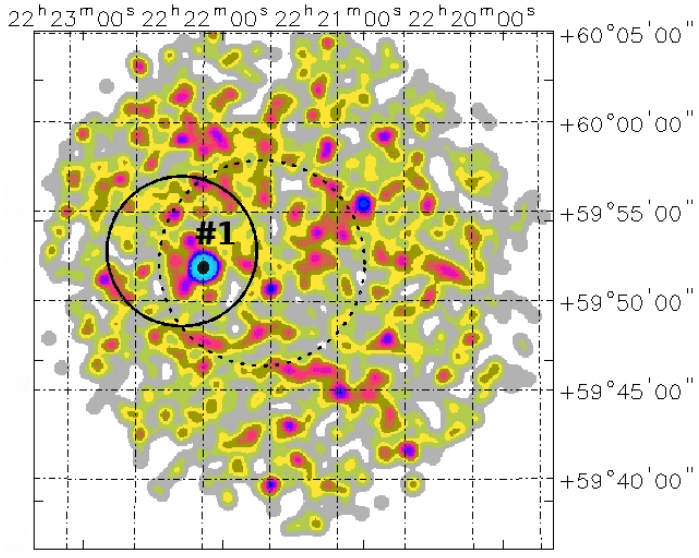

Figure 13: XRT 0.3–10 keV image of the region surrounding SWIFT J2221.6+5952. The XRT detection lies inside both the IBIS and BAT error circles (continuous and dotted black circles, respectively).

3.10. SWIFT J2221.6+5952

This source is another hard X-ray emitter that was listed for the first time in the 105-month *Swift*/BAT catalogue (Oh et al., 2018) and now reported also in the latest *INTEGRAL*/IBIS survey (Krivonos et al., 2022) as a source of unknown type (see Figure 13). SWIFT J2221.6+5952 was observed by XRT on various occasions over the period July 2015 and October 2016 (see Table A.1). From the analysis of each XRT measurements we can infer a 2–10 keV flux variability by a factor of ∼4 on a yearly time scale. However, due to the low statistical quality of the spectrum of each single pointing, we decided to stack all the observations together and perform the spectral analysis of the average spectrum, which can be modelled either with our basic model ($\Gamma \sim 0.9$) or with an absorbed power law ($N_{\rm H(intr)} \sim 0.8 \times 10^{22}$ cm^{-2}) if a canonical photon index of 1.8 is assumed (see Table 2).

Within the soft X-ray positional uncertainty no counterpart is found in any waveband enquired, which makes this object a peculiar high-energy emitter, especially for a source that is located on the Galactic plane. In radio, the upper limit is below the mJy level at a few GHz (see Table B.1), while in optical/IR the source is not visible to a level of 17 and 20 magnitudes in J and in B band, as inferred from the Two Micron All Sky Survey (2MASS, Skrutskie et al. 2006) and from the United States Naval Observatory (USNO–B1.0, Monet et al. 2003) catalogue, respectively.

The ratio of X-ray to optical fluxes is thus greater than 10, which may give some clues to the source nature. Indeed, although there is considerable dispersion, the most X-ray luminous (relative to optical) normal stars, normal galaxies, quasars, and BL Lac objects are known to have $log(f_x/f_{opt})$ of about –1, –0.25, 1.0, and 1.5, respectively (e.g., Stocke et al. 1991). This suggests an extragalactic nature for the source rather than a Galactic one.

SWIFT J2221.6+5952 is placed in the Cepheus constellation: this region is known to harbour intense star formation and various molecular clouds (Kun et al., 2008). It is also known for hiding background galaxies since Hubble (1934) first noted that in this region the zone of avoidance extends towards high Galactic latitudes. It is therefore possible that a background radio quiet AGN remains hidden in this region at optical/IR wavelengths and is only visible at high energies.

Although difficult, given the source location, we nevertheless encourage further multi-band follow-up observations possibly with high-sensitivity telescopes in order to establish the nature of this source.

4. Conclusions

X-ray observations play a key role to reduce the positional uncertainty associated with unidentified, often newly discovered, soft γ-ray sources, though favouring the search of their likely counterpart/s, and finally unveiling their, often complex, nature.

On the other hand, because of the crowdedness of the Galactic plane at optical/IR wavelengths, we expect to find many objects falling within the X-ray positional uncertainty, thus making the identification of a single/double counterpart at this wavelengths difficult. Often a multi-waveband/multi-archive approach, as used in the present study, can help in the process, but unfortunately it is not always resolutive. Furthermore, variability also needs to be taken into account, since objects seen occasionally by

Table 4: Summary of the proposed counterparts.

Source	Type
IGR J16173−5023	Galactic (CV)
IGR J16267−3303	Extragalactic (BL Lac)
IGR J17315−3221	Galactic
IGR J17327−4405	Galactic
IGR J17449−3037	Galactic (X-ray binary?)
IGR J17596−2315	Galactic
IGR J18006−3426	Blazar (FSRQ)
IGR J19071+0716	Galactic ?
IGR J19193+0754	Galactic (RS Canum Venaticorum ?)
SWIFT J2221.6+5952	Extragalactic ?

high-energy instruments, may not be bright enough during follow-up at lower energies and vice versa. In view of this, it is useful to analyse data taken by different instruments at different epochs, such as done in this work where *Swift*/XRT, *XMM-Newton* and *Chandra* observations were compared. Still despite this overall effort, the identification of high-energy sources on the Galactic plane remains a difficult task, as demonstrated in the present study.

The result of our work is summarised in Table 4, where we provide, for each high-energy emitter, a tentative classification on the basis of the all information gathered. For IGR J16173−5023, IGR J17315−3221, IGR J17449−3037, IGR J17596−2315, and IGR J19071+0716, the more accurate position provided either by *Swift*XRT, *XMM-Newton*, or *Chandra* enabled us to pinpoint a unique optical and/or IR counterpart. In the case of IGR J17327−4405, IGR J18006−3426, and IGR J19193+0754, the X-ray positional uncertainty is still too large to draw a firm conclusion about their optical/IR counterpart. For IGR J16267−3303, we found that the high-energy emission is most likely due to the contribution of two objects, which may be both classified as BL Lac. Our data also indicate that IGR J16173−5023 is likely a CV, IGR J17449−3037 a Galactic X-ray binary, IGR J18006−3426 a FSRQ-type Blazar, and IGR J19193+0754 a RS Canum Venaticorum system; IGR J17315−3221, IGR J17327−4405, IGR J17596−2315 and possibly IGR J19071+0716 are Galactic objects, although their specific optical class could not be assessed. In the case of SWIFT J2221.6+5952, no radio/optical/IR information is found for the X-ray counterpart, which makes this object peculiar also due to its location on the Galactic plane. Finally, two sources of the sample (IGR J17449−3037 and IGR J17596−2315) are positionally associated with the *Fermi*/LAT unidentified sources 2FHL J1745.1−3035 and 4FGL J1759.5−2312, respectively; thus, the identification/classification of these GeV sources is a useful by-product of the present work.

As a final remark, we wish to highlight that follow-up observations with current X-ray telescopes combined with multi-waveband studies (in particular optical/IR spectroscopy) are a powerful, but not always decisive, tool to assess the nature of unidentified high-energy emitter in the absence of better high-energy positioning capability.

Acknowledgements

We acknowledge the anonymous referee for his/her valuable comments. The authors acknowledge financial support from ASI under contract n. 2019-35-HH.0. This research has made use of data obtained from the VizieR catalog access tool and the SIMBAD database, which are both operated at CDS, Strasbourg, France; the NASA/IPAC Extragalactic Database (NED), which is operated by the Jet Propulsion Laboratory, California Institute of Technology, under contract with the National Aeronautics and Space Administration. This work has made use of data from the European Space Agency (ESA) mission *Gaia* (https://www.cosmos.esa.int/gaia), processed by the *Gaia* Data Processing and Analysis Consortium (DPAC, https://www.cosmos.esa.int/web/gaia/dpac/consortium). Funding for the DPAC has been provided by national institutions, in particular the institutions participating in the *Gaia* Multilateral Agreement. This paper exploited data from *XMM-Newton*, an ESA science mission with instruments and contributions directly funded by the ESA Member States and NASA. We also acknowledge the use of public data from the *Swift* data archive.

Appendix A. Log of the observations analysed in this paper

In this Appendix we report the log of the observations used in this work.

Table A.1: Log of the *Swift*/XRT and *XMM-Newton* observations used in this work. The exposure is expressed as net count rate.

IBIS source	ID	Obs date	Exposure (sec)	Instrument
IGR J16173−5023	00042853001	May 31, 2012	489	XRT
	00042853002	Jun 01, 2012	312	XRT
	00087349001	Apr 29, 2017	4810	XRT
	00041220001	Jan 14, 2019	1049	XRT
IGR J16267−3303	00015479001	Jan 20, 2023	2068	XRT
	00096647001	Jan 22, 2023	1838	XRT
IGR J17315−3221	00043517001	Sep 01, 2012	247	XRT
	00034659002	Aug 08, 2016	1144	XRT
	00034659003	Aug 10, 2016	1603	XRT
	00034659004	Aug 11, 2016	969	XRT
	00034659005	Aug 12, 2016	1064	XRT
	00034659006	Aug 15, 2016	1066	XRT
	00034659007	Aug 16, 2016	966	XRT
	00034659009	Aug 18, 2016	1029	XRT
	00034659010	Aug 19, 2016	1083	XRT
	00034659011	Aug 20, 2016	1056	XRT
	0886040101	Sep 14, 2022	13730	XMM
IGR J17327−4405	00085657001	Apr 17, 2017	782	XRT
	00085657002	Oct 24, 2017	240	XRT
	00085657003	Mar 09, 2018	4595	XRT
	00087157001	Jan 30, 2019	967	XRT
	00085657004	Jan 31, 2019	1086	XRT
	00087157002	Feb 01, 2019	974	XRT
	00085657005	Feb 27, 2019	1079	XRT
	00085657006	May 19, 2021	609	XRT
	00087157003	May 22, 2021	752	XRT
	00087157004	May 24, 2021	614	XRT
IGR J17449−3037	00043600001	Apr 22, 2012	784	XRT
	00093484002	Apr 13, 2017	62	XRT
	00093484003	Apr 20, 2017	35	XRT
	00093484004	May 04, 2017	57	XRT
	00093484005	May 18, 2017	55	XRT
	00093484006	Jun 01, 2017	55	XRT
	00093484007	Jun 15, 2017	48	XRT
	00093488007	Jun 15, 2017	50	XRT
	00093484008	Jun 23, 2017	57	XRT
	00089069001	Oct 30, 2020	1628	XRT

IBIS source	ID	Obs date	Exposure (sec)	Instrument
	00089069002	Apr 05, 2021	1600	XRT
	00089069003	Apr 07, 2021	1970	XRT
	0103261301	Mar 21, 2001	3864	XMM
	0782170601	Apr 03, 2017	5971	XMM
	0886010401	Mar 16, 2021	15360	XMM
IGR J17596−2315	00043799001	Feb 07, 2011	420	XRT
	00049688001	Feb 06, 2014	959	XRT
	00049688002	Aug 13, 2014	799	XRT
	00049688004	Nov 03, 2014	460	XRT
	00049688005	Feb 06, 2019	432	XRT
	0135742201	Mar 19, 2003	6866	XMM
	0135742301	Mar 20, 2003	6869	XMM
IGR J18006−3426	00091419001	Feb 02, 2013	934	XRT
	00091419002	Feb 08, 2013	2225	XRT
	00015480001	Feb 06, 2023	1895	XRT
IGR J19071+0716	00041804001	Nov 19, 2010	10673	XRT
	00044776001	Feb 17, 2012	1111	XRT
	00044775001	Mar 07, 2013	450	XRT
	00088696001	May 25, 2019	2095	XRT
	03109633001	Nov 28, 2019	167	XRT
	03109633002	Nov 30, 2019	170	XRT
	03109633003	Dec 02, 2019	125	XRT
	03109633004	Dec 03, 2019	355	XRT
	03109633005	Feb 21, 2020	899	XRT
	03109633006	Mar 02, 2020	812	XRT
	03109633007	Mar 09, 2020	981	XRT
IGR J19193+0754	00015470001	Feb 20, 2023	1910	XRT
SWIFT J2221.6+5952	00085697001	Jul 02, 2015	236	XRT
	00085697002	J ul 27, 2015	1073	XRT
	00085697003	Oct 08, 2015	607	XRT
	00085697004	Oct 09, 2015	549	XRT
	00085697005	Oct 25, 2015	356	XRT
	00085697006	Apr 04, 2016	2447	XRT
	00085697007	Apr 12, 2016	243	XRT
	00085697008	Jul 08, 2016	514	XRT
	00085697009	Jul 17, 2016	960	XRT
	00085697010	Jul 25, 2016	228	XRT
	00085697011	Aug 28, 2016	589	XRT
	00085697013	Oct 23, 2016	900	XRT

Appendix B. Radio Data

Table B.1: Radio data of the likely counterparts to the IBIS sources studied in this work.

Source	RACS[a] (mJy)	NVSS (mJy)	VLASS[a] (mJy)
	IGR J16173−5023		
#1	< 6.0	–	–
	IGR J16267−3303		
#1 and #2	< 0.79	–	< 0.56
	IGR J17315−3221		
#1	–	–	< 0.52
	IGR J17327−4405		
#1	< 0.84	–	–
	IGR J17449−3037		
#1	< 3.9	–	< 0.45
	IGR J17596−2315		
#1	–	–	< 0.61
	IGR J18006−3426		
#1	7.85 ± 0.30	2.90 ± 0.60	2.39 ± 0.26
	IGR J19071+0716		
#1	< 3.0	–	< 0.38
	IGR J19193+0754		
#1	< 1.5	–	< 0.72
	SWIFT J2221.6+5952		
#1	–	–	< 0.35

[a]: Upper limits are at 3σ confidence level.

In order to search for radio emission for the entire sample, we consulted recent all-sky surveys like the VLA Sky Survey at 3 GHz (VLASS, McConnell et al. 2020), and the Rapid ASKAP Continuum Survey at 0.88 GHz (RACS, Lacy et al. 2020). The images for the fields of interest were downloaded and analysed with the `CASA`[8] software (CASA Team et al., 2022). Flux densities were extracted through Gaussian fitting, except for the only resolved source NVSS J175948-230944, for which we estimated the flux density in VLASS considering a region that included the entire source. In case of non-detection, the image RMS was estimated in a region centered on source coordinates. The radio flux densities obtained from all these surveys are listed in Table B.1, which also specifies the database used. Inspection of Table B.1 indicates that most objects are not radio emitters with 3σ flux upper limits of the order of the mJy.

As expected, the only source detected (IGR J18006−3426) is an AGN (see dedicated section for further details). On the other hand, neither of the possible AGN counterparts to IGR J16267−3303 is detected at a flux limit of a fraction of a mJy, thus making the *WISE* colours the only signature of an extragalactic nature for this source.

[8]available at: https://casa.nrao.edu/

References

Abdollahi, S., Acero, F., Baldini, L., Ballet, J., Bastieri, D., Bellazzini, R., Berenji, B., Berretta, A., Bissaldi, E., Blandford, R.D., Bloom, E., Bonino, R., Brill, A., Britto, R.J., Bruel, P., Burnett, T.H., Buson, S., Cameron, R.A., Caputo, R., Caraveo, P.A., Castro, D., Chaty, S., Cheung, C.C., Chiaro, G., Cibrario, N., Ciprini, S., Coronado-Blázquez, J., Crnogorcevic, M., Cutini, S., D'Ammando, F., De Gaetano, S., Digel, S.W., Di Lalla, N., Dirirsa, F., Di Venere, L., Domínguez, A., Fallah Ramazani, V., Fegan, S.J., Ferrara, E.C., Fiori, A., Fleischhack, H., Franckowiak, A., Fukazawa, Y., Funk, S., Fusco, P., Galanti, G., Gammaldi, V., Gargano, F., Garrappa, S., Gasparrini, D., Giacchino, F., Giglietto, N., Giordano, F., Giroletti, M., Glanzman, T., Green, D., Grenier, I.A., Grondin, M.H., Guillemot, L., Guiriec, S., Gustafsson, M., Harding, A.K., Hays, E., Hewitt, J.W., Horan, D., Hou, X., Jóhannesson, G., Karwin, C., Kayanoki, T., Kerr, M., Kuss, M., Landriu, D., Larsson, S., Latronico, L., Lemoine-Goumard, M., Li, J., Liodakis, I., Longo, F., Loparco, F., Lott, B., Lubrano, P., Maldera, S., Malyshev, D., Manfreda, A., Martí-Devesa, G., Mazziotta, M.N., Mereu, I., Meyer, M., Michelson, P.F., Mirabal, N., Mitthumsiri, W., Mizuno, T., Moiseev, A.A., Monzani, M.E., Morselli, A., Moskalenko, I.V., Negro, M., Nuss, E., Omodei, N., Orienti, M., Orlando, E., Paneque, D., Pei, Z., Perkins, J.S., Persic, M., Pesce-Rollins, M., Petrosian, V., Pillera, R., Poon, H., Porter, T.A., Principe, G., Rainò, S., Rando, R., Rani, B., Razzano, M., Razzaque, S., Reimer, A., Reimer, O., Reposeur, T., Sánchez-Conde, M., Saz Parkinson, P.M., Scotton, L., Serini, D., Sgrò, C., Siskind, E.J., Smith, D.A., Spandre, G., Spinelli, P., Sueoka, K., Suson, D.J., Tajima, H., Tak, D., Thayer, J.B., Thompson, D.J., Torres, D.F., Troja, E., Valverde, J., Wood, K., Zaharijas, G., 2022. Incremental Fermi Large Area Telescope Fourth Source Catalog. Astrophys. J. Suppl. Ser. 260, 53. doi:10.3847/1538-4365/ac6751, arXiv:2201.11184.

Abril, J., Schmidtobreick, L., Ederoclite, A., López-Sanjuan, C., 2020. Disentangling cataclysmic variables in Gaia's HR diagram. Mon. Not. R. Astron. Soc. 492, L40–L44. doi:10.1093/mnrasl/slz181, arXiv:1912.01531.

Ackermann, M., Ajello, M., Atwood, W.B., Baldini, L., Ballet, J., Barbiellini, G., Bastieri, D., Becerra Gonzalez, J., Bellazzini, R., Bissaldi, E., Blandford, R.D., Bloom, E.D., Bonino, R., Bottacini, E., Brandt, T.J., Bregeon, J., Bruel, P., Buehler, R., Buson, S., Caliandro, G.A., Cameron, R.A., Caputo, R., Caragiulo, M., Caraveo, P.A., Cavazzuti, E., Cecchi, C., Charles, E., Chekhtman, A., Cheung, C.C., Chiang, J., Chiaro, G., Ciprini, S., Cohen, J.M., Cohen-Tanugi, J., Cominsky, L.R., Conrad, J., Cuoco, A., Cutini, S., D'Ammando, F., de Angelis, A., de Palma, F., Desiante, R., Di Mauro, M., Di Venere, L., Domínguez, A., Drell, P.S., Favuzzi, C., Fegan, S.J., Ferrara, E.C., Focke, W.B., Fortin, P., Franckowiak, A., Fukazawa, Y., Funk, S., Furniss, A.K., Fusco, P., Gargano, F., Gasparrini, D., Giglietto, N., Giommi, P., Giordano, F., Giroletti, M., Glanzman, T., Godfrey, G., Grenier, I.A., Grondin, M.H., Guillemot, L., Guiriec, S., Harding, A.K., Hays, E., Hewitt, J.W., Hill, A.B., Horan, D., Iafrate, G., Hartmann, D., Jogler, T., Jóhannesson, G., Johnson, A.S., Kamae, T., Kataoka, J., Knödlseder, J., Kuss, M., La Mura, G., Larsson, S., Latronico, L., Lemoine-Goumard, M., Li, J., Li, L., Longo, F., Loparco, F., Lott, B., Lovellette, M.N., Lubrano, P., Madejski, G.M., Maldera, S., Manfreda, A., Mayer, M., Mazziotta, M.N., Michelson, P.F., Mirabal, N., Mitthumsiri, W., Mizuno, T., Moiseev, A.A., Monzani, M.E., Morselli, A., Moskalenko, I.V., Murgia, S., Nuss, E., Ohsugi, T., Omodei, N., Orienti, M., Orlando, E., Ormes, J.F., Paneque, D., Perkins, J.S., Pesce-Rollins, M., Petrosian, V., Piron, F., Pivato, G., Porter, T.A., Rainò, S., Rando, R., Razzano, M., Razzaque, S., Reimer, A., Reimer, O., Reposeur, T., Romani, R.W., Sánchez-Conde, M., Saz Parkinson, P.M., Schmid, J., Schulz, A., Sgrò, C., Siskind, E.J., Spada, F., Spandre, G., Spinelli, P., Suson, D.J., Tajima, H., Takahashi, H., Takahashi, M., Takahashi, T., Thayer, J.B., Thompson, D.J., Tibaldo, L., Torres, D.F., Tosti, G., Troja, E., Vianello, G., Wood, K.S., Wood, M., Yassine, M., Zaharijas, G., Zimmer, S., 2016. 2FHL: The Second Catalog of Hard Fermi-LAT Sources. Astrophys. J. Suppl. Ser. 222, 5. doi:10.3847/0067-0049/222/1/5, arXiv:1508.04449.

Aharonian, F., Akhperjanian, A.G., Barres de Almeida, U., Bazer-Bachi, A.R., Behera, B., Beilicke, M., Benbow, W., Bernlöhr, K., Boisson, C., Bolz, O., Borrel, V., Braun, I., Brion, E., Brown, A.M., Bühler, R., Bulik, T., Büsching, I., Boutelier, T., Carrigan, S., Chadwick, P.M., Chounet, L.M., Clapson, A.C., Coignet, G., Cornils, R., Costamante, L., Dalton, M., Degrange, B., Dickinson, H.J., Djannati-Ataï, A., Domainko, W., O'C. Drury, L., Dubois, F., Dubus, G., Dyks, J., Egberts, K., Emmanoulopoulos, D., Espigat, P., Farnier, C., Feinstein, F., Fiasson, A., Förster, A., Fontaine, G., Funk, S., Füßling, M., Gallant, Y.A., Giebels, B., Glicenstein, J.F., Glück, B., Goret, P., Hadjichristidis, C., Hauser, D., Hauser, M., Heinzelmann, G., Henri, G., Hermann, G., Hinton, J.A., Hoffmann, A., Hofmann, W., Holleran, M., Hoppe, S., Horns, D., Jacholkowska, A., de Jager, O.C., Jung, I., Katarzyński, K., Kendziorra, E., Kerschhaggl, M., Khélifi, B., Keogh, D., Komin, N., Kosack, K., Lamanna, G., Latham, I.J., Lemoine-Goumard, M., Lenain, J.P., Lohse, T., Martin, J.M., Martineau-Huynh, O., Marcowith, A., Masterson, C., Maurin, D., McComb, T.J.L., Moderski, R., Moulin, E., Naumann-Godo, M., de Naurois, M., Nedbal, D., Nekrassov, D., Nolan, S.J., Ohm, S., Olive, J.P., de Oña Wilhelmi, E., Orford, K.J., Osborne, J.L., Ostrowski, M., Panter, M., Pedaletti, G., Pelletier, G., Petrucci, P.O., Pita, S., Pühlhofer, G., Punch, M., Raubenheimer, B.C., Raue, M., Rayner, S.M., Renaud, M., Ripken, J., Rob, L., Rosier-Lees, S., Rowell, G., Rudak, B., Ruppel, J., Sahakian, V., Santangelo, A., Schlickeiser, R., Schöck, F.M., Schröder, R., Schwanke, U., Schwarzburg, S., Schwemmer, S., Shalchi, A., Sol, H., Spangler, D., Stawarz, Ł., Steenkamp, R., Stegmann, C., Superina, G., Tam, P.H., Tavernet, J.P., Terrier, R., van Eldik, C., Vasileiadis, G., Venter, C., Vialle, J.P., Vincent, P., Vivier, M., Völk, H.J., Volpe, F., Wagner, S.J., Ward, M., Zdziarski, A.A., Zech, A., 2008. Exploring a SNR/molecular cloud association within HESS J1745-303. Astron. & Astrophys. 483, 509–517. doi:10.1051/0004-6361:20079230, arXiv:0803.2844.

Arnaud, K.A., 1996. XSPEC: The First Ten Years, in: Jacoby, G.H., Barnes, J. (Eds.), Astronomical Data Analysis Software and Systems V, p. 17.

Bailer-Jones, C.A.L., Rybizki, J., Fouesneau, M., Mantelet, G., Andrae, R., 2018. Estimating Distance from Parallaxes. IV. Distances to 1.33 Billion Stars in Gaia Data Release 2. Astron. J. 156, 58. doi:10.3847/1538-3881/aacb21, arXiv:1804.10121.

Barthelmy, S.D., Barbier, L.M., Cummings, J.R., Fenimore, E.E., Gehrels, N., Hullinger, D., Krimm, H.A., Markwardt, C.B., Palmer, D.M., Parsons, A., Sato, G., Suzuki, M., Takahashi, T., Tashiro, M., Tueller, J., 2005. The Burst Alert Telescope (BAT) on the SWIFT Midex Mission. Space Sci. Rev. 120, 143–164. doi:10.1007/s11214-005-5096-3, arXiv:astro-ph/0507410.

Bird, A.J., Bazzano, A., Malizia, A., Fiocchi, M., Sguera, V., Bassani, L., Hill, A.B., Ubertini, P., Winkler, C., 2016. The IBIS Soft Gamma-Ray Sky after 1000 Integral Orbits. Astrophys. J. Suppl. Ser. 223, 15. doi:10.3847/0067-0049/223/1/15, arXiv:1601.06074.

Burrows, D.N., Hill, J.E., Nousek, J.A., Kennea, J.A., Wells, A., Osborne, J.P., Abbey, A.F., Beardmore, A., Mukerjee, K., Short, A.D.T., Chincarini, G., Campana, S., Citterio, O., Moretti, A., Pagani, C., Tagliaferri, G., Giommi, P., Capalbi, M., Tamburelli, F., Angelini, L., Cusumano, G., Bräuninger, H.W., Burkert, W., Hartner, G.D., 2005. The Swift X-Ray Telescope. Space Sci. Rev. 120, 165–195. doi:10.1007/s11214-005-5097-2, arXiv:astro-ph/0508071.

Butler, S.C., Tomsick, J.A., Chaty, S., Heras, J.A.Z., Rodriguez, J., Walter, R., Kaaret, P., Kalemci, E., Özbey, M., 2009. Identifications of Five INTEGRAL Sources via Optical Spectroscopy. Astrophys. J. 698, 502–508. doi:10.1088/0004-637X/698/1/502, arXiv:0903.1302.

CASA Team, Bean, B., Bhatnagar, S., Castro, S., Donovan Meyer, J., Emonts, B., Garcia, E., Garwood, R., Golap, K., Gonzalez Villalba, J., Harris, P., Hayashi, Y., Hoskins, J., Hsieh, M., Jagannathan, P., Kawasaki, W., Keimpema, A., Kettenis, M., Lopez,

J., Marvil, J., Masters, J., McNichols, A., Mehringer, D., Miel, R., Moellenbrock, G., Montesino, F., Nakazato, T., Ott, J., Petry, D., Pokorny, M., Raba, R., Rau, U., Schiebel, D., Schweighart, N., Sekhar, S., Shimada, K., Small, D., Steeb, J.W., Sugimoto, K., Suoranta, V., Tsutsumi, T., van Bemmel, I.M., Verkouter, M., Wells, A., Xiong, W., Szomoru, A., Griffith, M., Glendenning, B., Kern, J., 2022. CASA, the Common Astronomy Software Applications for Radio Astronomy. Publ. Astron. Soc. Pac. 134, 114501. doi:10.1088/1538-3873/ac9642, arXiv:2210.02276.

Cash, W., 1979. Parameter estimation in astronomy through application of the likelihood ratio. Astrophys. J. 228, 939–947. doi:10.1086/156922.

Chambers, K.C., Magnier, E.A., Metcalfe, N., Flewelling, H.A., Huber, M.E., Waters, C.Z., Denneau, L., Draper, P.W., Farrow, D., Finkbeiner, D.P., Holmberg, C., Koppenhoefer, J., Price, P.A., Rest, A., Saglia, R.P., Schlafly, E.F., Smartt, S.J., Sweeney, W., Wainscoat, R.J., Burgett, W.S., Chastel, S., Grav, T., Heasley, J.N., Hodapp, K.W., Jedicke, R., Kaiser, N., Kudritzki, R.P., Luppino, G.A., Lupton, R.H., Monet, D.G., Morgan, J.S., Onaka, P.M., Shiao, B., Stubbs, C.W., Tonry, J.L., White, R., Bañados, E., Bell, E.F., Bender, R., Bernard, E.J., Boegner, M., Boffi, F., Botticella, M.T., Calamida, A., Casertano, S., Chen, W.P., Chen, X., Cole, S., Deacon, N., Frenk, C., Fitzsimmons, A., Gezari, S., Gibbs, V., Goessl, C., Goggia, T., Gourgue, R., Goldman, B., Grant, P., Grebel, E.K., Hambly, N.C., Hasinger, G., Heavens, A.F., Heckman, T.M., Henderson, R., Henning, T., Holman, M., Hopp, U., Ip, W.H., Isani, S., Jackson, M., Keyes, C.D., Koekemoer, A.M., Kotak, R., Le, D., Liska, D., Long, K.S., Lucey, J.R., Liu, M., Martin, N.F., Masci, G., McLean, B., Mindel, E., Misra, P., Morganson, E., Murphy, D.N.A., Obaika, A., Narayan, G., Nieto-Santisteban, M.A., Norberg, P., Peacock, J.A., Pier, E.A., Postman, M., Primak, N., Rae, C., Rai, A., Riess, A., Riffeser, A., Rix, H.W., Röser, S., Russel, R., Rutz, L., Schilbach, E., Schultz, A.S.B., Scolnic, D., Strolger, L., Szalay, A., Seitz, S., Small, E., Smith, K.W., Soderblom, D.R., Taylor, P., Thomson, R., Taylor, A.N., Thakar, A.R., Thiel, J., Thilker, D., Unger, D., Urata, Y., Valenti, J., Wagner, J., Walder, T., Walter, F., Watters, S.P., Werner, S., Wood-Vasey, W.M., Wyse, R., 2016. The Pan-STARRS1 Surveys. arXiv e-prints , arXiv:1612.05560doi:10.48550/arXiv.1612.05560, arXiv:1612.05560.

Condon, J.J., Cotton, W.D., Greisen, E.W., Yin, Q.F., Perley, R.A., Taylor, G.B., Broderick, J.J., 1998. The NRAO VLA Sky Survey. Astron. J. 115, 1693–1716. doi:10.1086/300337.

Cutri, R.M., Wright, E.L., Conrow, T., Fowler, J.W., Eisenhardt, P.R.M., Grillmair, C., Kirkpatrick, J.D., Masci, F., McCallon, H.L., Wheelock, S.L., Fajardo-Acosta, S., Yan, L., Benford, D., Harbut, M., Jarrett, T., Lake, S., Leisawitz, D., Ressler, M.E., Stanford, S.A., Tsai, C.W., Liu, F., Helou, G., Mainzer, A., Gettngs, D., Gonzalez, A., Hoffman, D., Marsh, K.A., Padgett, D., Skrutskie, M.F., Beck, R., Papin, M., Wittman, M., 2021. VizieR Online Data Catalog: AllWISE Data Release (Cutri+ 2013). VizieR Online Data Catalog , II/328.

D'Abrusco, R., Álvarez Crespo, N., Massaro, F., Campana, R., Chavushyan, V., Landoni, M., La Franca, F., Masetti, N., Milisavljevic, D., Paggi, A., Ricci, F., Smith, H.A., 2019. Two New Catalogs of Blazar Candidates in the WISE Infrared Sky. Astrophys. J. Suppl. Ser. 242, 4. doi:10.3847/1538-4365/ab16f4, arXiv:1903.11124.

Drew, J.E., Gonzalez-Solares, E., Greimel, R., Irwin, M.J., Küpcü Yoldas, A., Lewis, J., Barentsen, G., Eislöffel, J., Farnhill, H.J., Martin, W.E., Walsh, J.R., Walton, N.A., Mohr-Smith, M., Raddi, R., Sale, S.E., Wright, N.J., Groot, P., Barlow, M.J., Corradi, R.L.M., Drake, J.J., Fabregat, J., Frew, D.J., Gänsicke, B.T., Knigge, C., Mampaso, A., Morris, R.A.H., Naylor, T., Parker, Q.A., Phillipps, S., Ruhland, C., Steeghs, D., Unruh, Y.C., Vink, J.S., Wesson, R., Zijlstra, A.A., 2014. The VST Photometric Hα Survey of the Southern Galactic Plane and Bulge (VPHAS+). Mon. Not. R. Astron. Soc. 440, 2036–2058. doi:10.1093/mnras/stu394, arXiv:1402.7024.

Ergin, T., Saha, L., Bhattacharjee, P., Sano, H., Tanaka, S.J., Majumdar, P., Yamazaki, R., Fukui, Y., 2021. Probing the star formation origin of gamma-rays from 3FHL J1907.0+0713. Mon. Not. R. Astron. Soc. 501, 4226–4237. doi:10.1093/mnras/staa3817, arXiv:2012.07357.

Evans, P.A., Page, K.L., Osborne, J.P., Beardmore, A.P., Willingale, R., Burrows, D.N., Kennea, J.A., Perri, M., Capalbi, M., Tagliaferri, G., Cenko, S.B., 2020. 2SXPS: An Improved and Expanded Swift X-Ray Telescope Point-source Catalog. Astrophys. J. Suppl. Ser. 247, 54. doi:10.3847/1538-4365/ab7db9, arXiv:1911.11710.

Fan, J.H., Chen, K.Y., Xiao, H.B., Yang, W.X., Liang, J.C., Chen, G.H., Yang, J.H., Yuan, Y.H., Wu, D.X., 2022. The Classification of Blazar Candidates of Uncertain Types. Universe 8, 436. doi:10.3390/universe8080436, arXiv:2208.12917.

Ferrigno, C., Bozzo, E., Romano, P., 2022. XMM-Newton and Swift observations of supergiant high mass X-ray binaries. Astron. & Astrophys. 664, A99. doi:10.1051/0004-6361/202243294, arXiv:2205.03023.

Gaia Collaboration, 2022. VizieR Online Data Catalog: Gaia DR3 Part 4. Variability (Gaia Collaboration, 2022). VizieR Online Data Catalog , I/358.

Gaia Collaboration, Brown, A.G.A., Vallenari, A., Prusti, T., de Bruijne, J.H.J., Babusiaux, C., Biermann, M., Creevey, O.L., Evans, D.W., Eyer, L., Hutton, A., Jansen, F., Jordi, C., Klioner, S.A., Lammers, U., Lindegren, L., Luri, X., Mignard, F., Panem, C., Pourbaix, D., Randich, S., Sartoretti, P., Soubiran, C., Walton, N.A., Arenou, F., Bailer-Jones, C.A.L., Bastian, U., Cropper, M., Drimmel, R., Katz, D., Lattanzi, M.G., van Leeuwen, F., Bakker, J., Cacciari, C., Castañeda, J., De Angeli, F., Ducourant, C., Fabricius, C., Fouesneau, M., Frémat, Y., Guerra, R., Guerrier, A., Guiraud, J., Jean-Antoine Piccolo, A., Masana, E., Messineo, R., Mowlavi, N., Nicolas, C., Nienartowicz, K., Pailler, F., Panuzzo, P., Riclet, F., Roux, W., Seabroke, G.M., Sordo, R., Tanga, P., Thévenin, F., Gracia-Abril, G., Portell, J., Teyssier, D., Altmann, M., Andrae, R., Bellas-Velidis, I., Benson, K., Berthier, J., Blomme, R., Brugaletta, E., Burgess, P.W., Busso, G., Carry, B., Cellino, A., Cheek, N., Clementini, G., Damerdji, Y., Davidson, M., Delchambre, L., Dell'Oro, A., Fernández-Hernández, J., Galluccio, L., García-Lario, P., Garcia-Reinaldos, M., González-Núñez, J., Gosset, E., Haigron, R., Halbwachs, J.L., Hambly, N.C., Harrison, D.L., Hatzidimitriou, D., Heiter, U., Hernández, J., Hestroffer, D., Hodgkin, S.T., Holl, B., Janßen, K., Jevardat de Fombelle, G., Jordan, S., Krone-Martins, A., Lanzafame, A.C., Löffler, W., Lorca, A., Manteiga, M., Marchal, O., Marrese, P.M., Moitinho, A., Mora, A., Muinonen, K., Osborne, P., Pancino, E., Pauwels, T., Petit, J.M., Recio-Blanco, A., Richards, P.J., Riello, M., Rimoldini, L., Robin, A.C., Roegiers, T., Rybizki, J., Sarro, L.M., Siopis, C., Smith, M., Sozzetti, A., Ulla, A., Utrilla, E., van Leeuwen, M., van Reeven, W., Abbas, U., Abreu Aramburu, A., Accart, S., Aerts, C., Aguado, J.J., Ajaj, M., Altavilla, G., Álvarez, M.A., Álvarez Cid-Fuentes, J., Alves, J., Anderson, R.I., Anglada Varela, E., Antoja, T., Audard, M., Baines, D., Baker, S.G., Balaguer-Núñez, L., Balbinot, E., Balog, Z., Barache, C., Barbato, D., Barros, M., Barstow, M.A., Bartolomé, S., Bassilana, J.L., Bauchet, N., Baudesson-Stella, A., Becciani, U., Bellazzini, M., Bernet, M., Bertone, S., Bianchi, L., Blanco-Cuaresma, S., Boch, T., Bombrun, A., Bossini, D., Bouquillon, S., Bragaglia, A., Bramante, L., Breedt, E., Bressan, A., Brouillet, N., Bucciarelli, B., Burlacu, A., Busonero, D., Butkevich, A.G., Buzzi, R., Caffau, E., Cancelliere, R., Cánovas, H., Cantat-Gaudin, T., Carballo, R., Carlucci, T., Carnerero, M.I., Carrasco, J.M., Casamiquela, L., Castellani, M., Castro-Ginard, A., Castro Sampol, P., Chaoul, L., Charlot, P., Chemin, L., Chiavassa, A., Cioni, M.R.L., Comoretto, G., Cooper, W.J., Cornez, T., Cowell, S., Crifo, F., Crosta, M., Crowley, C., Dafonte, C., Dapergolas, A., David, M., David, P., de Laverny, P., De Luise, F., De March, R., De Ridder, J., de Souza, R., de Teodoro, P., de Torres, A., del Peloso, E.F., del Pozo, E., Delbo, M., Delgado, A., Delgado, H.E., Delisle, J.B., Di Matteo, P., Diakite, S., Diener, C., Distefano, E., Dolding, C., Eappachen, D., Edvardsson, B., Enke, H., Esquej, P., Fabre, C., Fabrizio, M., Faigler, S., Fedorets, G., Fernique, P., Fienga, A., Figueras, F., Fouron, C., Fragkoudi, F., Fraile, E., Franke, F., Gai, M., Garabato, D., Garcia-Gutierrez, A., García-Torres, M., Garofalo,

A., Gavras, P., Gerlach, E., Geyer, R., Giacobbe, P., Gilmore, G., Girona, S., Giuffrida, G., Gomel, R., Gomez, A., Gonzalez-Santamaria, I., González-Vidal, J.J., Granvik, M., Gutiérrez-Sánchez, R., Guy, L.P., Hauser, M., Haywood, M., Helmi, A., Hidalgo, S.L., Hilger, T., Hładczuk, N., Hobbs, D., Holland, G., Huckle, H.E., Jasniewicz, G., Jonker, P.G., Juaristi Campillo, J., Julbe, F., Karbevska, L., Kervella, P., Khanna, S., Kochoska, A., Kontizas, M., Kordopatis, G., Korn, A.J., Kostrzewa-Rutkowska, Z., Kruszyńska, K., Lambert, S., Lanza, A.F., Lasne, Y., Le Campion, J.F., Le Fustec, Y., Lebreton, Y., Lebzelter, T., Leccia, S., Leclerc, N., Lecoeur-Taibi, I., Liao, S., Licata, E., Lindstrøm, E.P., Lister, T.A., Livanou, E., Lobel, A., Madrero Pardo, P., Managau, S., Mann, R.G., Marchant, J.M., Marconi, M., Marcos Santos, M.M.S., Marinoni, S., Marocco, F., Marshall, D.J., Martin Polo, L., Martín-Fleitas, J.M., Masip, A., Massari, D., Mastrobuono-Battisti, A., Mazeh, T., McMillan, P.J., Messina, S., Michalik, D., Millar, N.R., Mints, A., Molina, D., Molinaro, R., Molnár, L., Montegriffo, P., Mor, R., Morbidelli, R., Morel, T., Morris, D., Mulone, A.F., Munoz, D., Muraveva, T., Murphy, C.P., Musella, I., Noval, L., Ordénovic, C., Orrù, G., Osinde, J., Pagani, C., Pagano, I., Palaversa, L., Palicio, P.A., Panahi, A., Pawlak, M., Peñalosa Esteller, X., Penttilä, A., Piersimoni, A.M., Pineau, F.X., Plachy, E., Plum, G., Poggio, E., Poretti, E., Poujoulet, E., Prša, A., Pulone, L., Racero, E., Ragaini, S., Rainer, M., Raiteri, C.M., Rambaux, N., Ramos, P., Ramos-Lerate, M., Re Fiorentin, P., Regibo, S., Reylé, C., Ripepi, V., Riva, A., Rixon, G., Robichon, N., Robin, C., Roelens, M., Rohrbasser, L., Romero-Gómez, M., Rowell, N., Royer, F., Rybicki, K.A., Sadowski, G., Sagristà Sellés, A., Sahlmann, J., Salgado, J., Salguero, E., Samaras, N., Sanchez Gimenez, V., Sanna, N., Santoveña, R., Sarasso, M., Schultheis, M., Sciacca, E., Segol, M., Segovia, J.C., Ségransan, D., Semeux, D., Shahaf, S., Siddiqui, H.I., Siebert, A., Siltala, L., Slezak, E., Smart, R.L., Solano, E., Solitro, F., Souami, D., Souchay, J., Spagna, A., Spoto, F., Steele, I.A., Steidelmüller, H., Stephenson, C.A., Süveges, M., Szabados, L., Szegedi-Elek, E., Taris, F., Tauran, G., Taylor, M.B., Teixeira, R., Thuillot, W., Tonello, N., Torra, F., Torra, J., Turon, C., Unger, N., Vaillant, M., van Dillen, E., Vanel, O., Vecchiato, A., Viala, Y., Vicente, D., Voutsinas, S., Weiler, M., Wevers, T., Wyrzykowski, Ł., Yoldas, A., Yvard, P., Zhao, H., Zorec, J., Zucker, S., Zurbach, C., Zwitter, T., 2021. Gaia Early Data Release 3. Summary of the contents and survey properties. Astron. & Astrophys. 649, A1. doi:10.1051/0004-6361/202039657, arXiv:2012.01533.

Gaia Collaboration, Eyer, L., Rimoldini, L., Audard, M., Anderson, R.I., Nienartowicz, K., Glass, F., Marchal, O., Grenon, M., Mowlavi, N., Holl, B., Clementini, G., Aerts, C., Mazeh, T., Evans, D.W., Szabados, L., Brown, A.G.A., Vallenari, A., Prusti, T., de Bruijne, J.H.J., Babusiaux, C., Bailer-Jones, C.A.L., Biermann, M., Jansen, F., Jordi, C., Klioner, S.A., Lammers, U., Lindegren, L., Luri, X., Mignard, F., Panem, C., Pourbaix, D., Randich, S., Sartoretti, P., Siddiqui, H.I., Soubiran, C., van Leeuwen, F., Walton, N.A., Arenou, F., Bastian, U., Cropper, M., Drimmel, R., Katz, D., Lattanzi, M.G., Bakker, J., Cacciari, C., Castañeda, J., Chaoul, L., Cheek, N., De Angeli, F., Fabricius, C., Guerra, R., Masana, E., Messineo, R., Panuzzo, P., Portell, J., Riello, M., Seabroke, G.M., Tanga, P., Thévenin, F., Gracia-Abril, G., Comoretto, G., Garcia-Reinaldos, M., Teyssier, D., Altmann, M., Andrae, R., Bellas-Velidis, I., Benson, K., Berthier, J., Blomme, R., Burgess, P., Busso, G., Carry, B., Cellino, A., Clotet, M., Creevey, O., Davidson, M., De Ridder, J., Delchambre, L., Dell'Oro, A., Ducourant, C., Fernández-Hernández, J., Fouesneau, M., Frémat, Y., Galluccio, L., García-Torres, M., González-Núñez, J., González-Vidal, J.J., Gosset, E., Guy, L.P., Halbwachs, J.L., Hambly, N.C., Harrison, D.L., Hernández, J., Hestroffer, D., Hodgkin, S.T., Hutton, A., Jasniewicz, G., Jean-Antoine-Piccolo, A., Jordan, S., Korn, A.J., Krone-Martins, A., Lanzafame, A.C., Lebzelter, T., Löffler, W., Manteiga, M., Marrese, P.M., Martín-Fleitas, J.M., Moitinho, A., Mora, A., Muinonen, K., Osinde, J., Pancino, E., Pauwels, T., Petit, J.M., Recio-Blanco, A., Richards, P.J., Robin, A.C., Sarro, L.M., Siopis, C., Smith, M., Sozzetti, A., Süveges, M., Torra, J., van Reeven, W., Abbas, U., Abreu Aramburu, A., Accart, S., Altavilla, G., Álvarez, M.A., Alvarez, R., Alves, J., Andrei, A.H., Anglada Varela, E., Antiche, E., Antoja, T., Arcay, B., Astraatmadja, T.L., Bach, N., Baker, S.G., Balaguer-Núñez, L., Balm, P., Barache, C., Barata, C., Barbato, D., Barblan, F., Barklem, P.S., Barrado, D., Barros, M., Barstow, M.A., Bartholomé Muñoz, S., Bassilana, J.L., Becciani, U., Bellazzini, M., Berihuete, A., Bertone, S., Bianchi, L., Bienaymé, O., Blanco-Cuaresma, S., Boch, T., Boeche, C., Bombrun, A., Borrachero, R., Bossini, D., Bouquillon, S., Bourda, G., Bragaglia, A., Bramante, L., Breddels, M.A., Bressan, A., Brouillet, N., Brüsemeister, T., Brugaletta, E., Bucciarelli, B., Burlacu, A., Busonero, D., Butkevich, A.G., Buzzi, R., Caffau, E., Cancelliere, R., Cannizzaro, G., Cantat-Gaudin, T., Carballo, R., Carlucci, T., Carrasco, J.M., Casamiquela, L., Castellani, M., Castro-Ginard, A., Charlot, P., Chemin, L., Chiavassa, A., Cocozza, G., Costigan, G., Cowell, S., Crifo, F., Crosta, M., Crowley, C., Cuypers, J., Dafonte, C., Damerdji, Y., Dapergolas, A., David, P., David, M., de Laverny, P., De Luise, F., De March, R., de Martino, D., de Souza, R., de Torres, A., Debosscher, J., del Pozo, E., Delbo, M., Delgado, A., Delgado, H.E., Diakite, S., Diener, C., Distefano, E., Dolding, C., Drazinos, P., Durán, J., Edvardsson, B., Enke, H., Eriksson, K., Esquej, P., Eynard Bontemps, G., Fabre, C., Fabrizio, M., Faigler, S., Falcão, A.J., Farràs Casas, M., Federici, L., Fedorets, G., Fernique, P., Figueras, F., Filippi, F., Findeisen, K., Fonti, A., Fraile, E., Fraser, M., Frézouls, B., Gai, M., Galleti, S., Garabato, D., García-Sedano, F., Garofalo, A., Garralda, N., Gavel, A., Gavras, P., Gerssen, J., Geyer, R., Giacobbe, P., Gilmore, G., Girona, S., Giuffrida, G., Gomes, M., Granvik, M., Gueguen, A., Guerrier, A., Guiraud, J., Gutiérrez-Sánchez, R., Haigron, R., Hatzidimitriou, D., Hauser, M., Haywood, M., Heiter, U., Helmi, A., Heu, J., Hilger, T., Hobbs, D., Hofmann, W., Holland, G., Huckle, H.E., Hypki, A., Icardi, V., Janßen, K., Jevardat de Fombelle, G., Jonker, P.G., Juhász, Á.L., Julbe, F., Karampelas, A., Kewley, A., Klar, J., Kochoska, A., Kohley, R., Kolenberg, K., Kontizas, M., Kontizas, E., Koposov, S.E., Kordopatis, G., Kostrzewa-Rutkowska, Z., Koubsky, P., Lambert, S., Lanza, A.F., Lasne, Y., Lavigne, J.B., Le Fustec, Y., Le Poncin-Lafitte, C., Lebreton, Y., Leccia, S., Leclerc, N., Lecoeur-Taibi, I., Lenhardt, H., Leroux, F., Liao, S., Licata, E., Lindstrøm, H.E.P., Lister, T.A., Livanou, E., Lobel, A., López, M., Lorenz, D., Managau, S., Mann, R.G., Mantelet, G., Marchant, J.M., Marconi, M., Marinoni, S., Marschalkó, G., Marshall, D.J., Martino, M., Marton, G., Mary, N., Massari, D., Matijevič, G., McMillan, P.J., Messina, S., Michalik, D., Millar, N.R., Molina, D., Molinaro, R., Molnár, L., Montegriffo, P., Mor, R., Morbidelli, R., Morel, T., Morgenthaler, S., Morris, D., Mulone, A.F., Muraveva, T., Musella, I., Nelemans, G., Nicastro, L., Noval, L., O'Mullane, W., Ordénovic, C., Ordóñez-Blanco, D., Osborne, P., Pagani, C., Pagano, I., Pailler, F., Palacin, H., Palaversa, L., Panahi, A., Pawlak, M., Piersimoni, A.M., Pineau, F.X., Plachy, E., Plum, G., Poggio, E., Poujoulet, E., Prša, A., Pulone, L., Racero, E., Ragaini, S., Rambaux, N., Ramos-Lerate, M., Regibo, S., Reylé, C., Riclet, F., Ripepi, V., Riva, A., Rivard, A., Rixon, G., Roegiers, T., Roelens, M., Romero-Gómez, M., Rowell, N., Royer, F., Ruiz-Dern, L., Sadowski, G., Sagristà Sellés, T., Sahlmann, J., Salgado, J., Salguero, E., Sanna, N., Santana-Ros, T., Sarasso, M., Savietto, H., Schultheis, M., Sciacca, E., Segol, M., Segovia, J.C., Ségransan, D., Shih, I.C., Siltala, L., Silva, A.F., Smart, R.L., Smith, K.W., Solano, E., Solitro, F., Sordo, R., Soria Nieto, S., Souchay, J., Spagna, A., Spoto, F., Stampa, U., Steele, I.A., Steidelmüller, H., Stephenson, C.A., Stoev, H., Suess, F.F., Surdej, J., Szegedi-Elek, E., Tapiador, D., Taris, F., Tauran, G., Taylor, M.B., Teixeira, R., Terrett, D., Teyssandier, P., Thuillot, W., Titarenko, A., Torra Clotet, F., Turon, C., Ulla, A., Utrilla, E., Uzzi, S., Vaillant, M., Valentini, G., Valette, V., van Elteren, A., Van Hemelryck, E., van Leeuwen, M., Vaschetto, M., Vecchiato, A., Veljanoski, J., Viala, Y., Vicente, D., Vogt, S., von Essen, C., Voss, H., Votruba, V., Voutsinas, S., Walmsley, G., Weiler, M., Wertz, O., Wevers, T., Wyrzykowski, Ł., Yoldas, A., Žerjal, M., Ziaeepour, H., Zorec, J., Zschocke, S., Zucker, S., Zurbach, C., Zwitter, T., 2019. Gaia Data Release 2. Variable stars in the

colour-absolute magnitude diagram. Astron. & Astrophys. 623, A110. doi:10.1051/0004-6361/201833304, arXiv:1804.09382.

Haakonsen, C.B., Rutledge, R.E., 2009. XID II: Statistical Cross-Association of ROSAT Bright Source Catalog X-ray Sources with 2MASS Point Source Catalog Near-Infrared Sources. Astrophys. J. Suppl. Ser. 184, 138–151. doi:10.1088/0067-0049/184/1/138, arXiv:0910.3229.

Hill, J., Burrows, D., Nousek, J., Wells, A., Osborne, J., Mukerjee, K., Chincarini, G., Tagliaferri, G., Campana, S., 2004. The Swift X-ray Telescope, in: APS April Meeting Abstracts, p. S10.005.

Hubble, E., 1934. The Distribution of Extra-Galactic Nebulae. Astrophys. J. 79, 8. doi:10.1086/143517.

Kalberla, P.M.W., Dedes, L., Arnal, E.M., Bajaja, E., Morras, R., Pöppel, W.G.L., 2005. Extra-planar Gas in the Leiden/Argentine/Bonn HI Survey, in: Braun, R. (Ed.), Extra-Planar Gas, p. 81.

Karasev, D.I., Lutovinov, A.A., Tkachenko, A.Y., Khorunzhev, G.A., Krivonos, R.A., Medvedev, P.S., Pavlinsky, M.N., Burenin, R.A., Eselevich, M.V., 2018. Optical Identification of X-ray Sources from the 14-Year INTEGRAL All-Sky Survey. Astronomy Letters 44, 522–540. doi:10.1134/S1063773718090037, arXiv:1809.02949.

Kiraga, M., 2012. ASAS Photometry of ROSAT Sources. I. Periodic Variable Stars Coincident with Bright Sources from the ROSAT All Sky Survey. Acta Astron. 62, 67–95. doi:10.48550/arXiv.1204.3825, arXiv:1204.3825.

Koss, M., Trakhtenbrot, B., Ricci, C., Lamperti, I., Oh, K., Berney, S., Schawinski, K., Baloković, M., Baronchelli, L., Crenshaw, D.M., Fischer, T., Gehrels, N., Harrison, F., Hashimoto, Y., Hogg, D., Ichikawa, K., Masetti, N., Mushotzky, R., Sartori, L., Stern, D., Treister, E., Ueda, Y., Veilleux, S., Winter, L., 2017. BAT AGN Spectroscopic Survey. I. Spectral Measurements, Derived Quantities, and AGN Demographics. Astrophys. J. 850, 74. doi:10.3847/1538-4357/aa8ec9, arXiv:1707.08123.

Krivonos, R., Revnivtsev, M., Lutovinov, A., Sazonov, S., Churazov, E., Sunyaev, R., 2007. INTEGRAL/IBIS all-sky survey in hard X-rays. Astron. & Astrophys. 475, 775–784. doi:10.1051/0004-6361:20077191, arXiv:astro-ph/0701836.

Krivonos, R., Tsygankov, S., Lutovinov, A., Revnivtsev, M., Churazov, E., Sunyaev, R., 2012. INTEGRAL/IBIS nine-year Galactic hard X-ray survey. Astron. & Astrophys. 545, A27. doi:10.1051/0004-6361/201219617, arXiv:1205.3941.

Krivonos, R.A., Sazonov, S.Y., Kuznetsova, E.A., Lutovinov, A.A., Mereminskiy, I.A., Tsygankov, S.S., 2022. INTEGRAL/IBIS 17-yr hard X-ray all-sky survey. Mon. Not. R. Astron. Soc. 510, 4796–4807. doi:10.1093/mnras/stab3751, arXiv:2111.02996.

Krivonos, R.A., Tsygankov, S.S., Mereminskiy, I.A., Lutovinov, A.A., Sazonov, S.Y., Sunyaev, R.A., 2017. New hard X-ray sources discovered in the ongoing INTEGRAL Galactic plane survey after 14 yr of observations. Mon. Not. R. Astron. Soc. 470, 512–516. doi:10.1093/mnras/stx1276, arXiv:1704.03364.

Kun, M., Kiss, Z.T., Balog, Z., 2008. Star Forming Regions in Cepheus, in: Reipurth, B. (Ed.), Handbook of Star Forming Regions, Volume I. volume 4, p. 136. doi:10.48550/arXiv.0809.4761.

Lacy, M., Baum, S.A., Chandler, C.J., Chatterjee, S., Clarke, T.E., Deustua, S., English, J., Farnes, J., Gaensler, B.M., Gugliucci, N., Hallinan, G., Kent, B.R., Kimball, A., Law, C.J., Lazio, T.J.W., Marvil, J., Mao, S.A., Medlin, D., Mooley, K., Murphy, E.J., Myers, S., Osten, R., Richards, G.T., Rosolowsky, E., Rudnick, L., Schinzel, F., Sivakoff, G.R., Sjouwerman, L.O., Taylor, R., White, R.L., Wrobel, J., Andernach, H., Beasley, A.J., Berger, E., Bhatnager, S., Birkinshaw, M., Bower, G.C., Brandt, W.N., Brown, S., Burke-Spolaor, S., Butler, B.J., Comerford, J., Demorest, P.B., Fu, H., Giacintucci, S., Golap, K., Güth, T., Hales, C.A., Hiriart, R., Hodge, J., Horesh, A., Ivezić, Ž., Jarvis, M.J., Kamble, A., Kassim, N., Liu, X., Loinard, L., Lyons, D.K., Masters, J., Mezcua, M., Moellenbrock, G.A., Mroczkowski, T., Nyland, K., O'Dea, C.P., O'Sullivan, S.P., Peters, W.M., Radford, K., Rao, U., Robnett, J., Salcido, J., Shen, Y., Sobotka, A., Witz, S., Vaccari, M., van Weeren, R.J., Vargas, A., Williams, P.K.G., Yoon, I., 2020. The Karl G. Jansky Very Large Array Sky Survey (VLASS). Science Case and Survey Design. Publ. Astron. Soc. Pac. 132, 035001. doi:10.1088/1538-3873/ab63eb, arXiv:1907.01981.

Landi, R., Bassani, L., Dean, A.J., Bird, A.J., Fiocchi, M., Bazzano, A., Nousek, J.A., Osborne, J.P., 2009. INTEGRAL/IBIS and Swift/XRT observations of hard cataclysmic variables. Mon. Not. R. Astron. Soc. 392, 630–640. doi:10.1111/j.1365-2966.2008.14086.x, arXiv:0810.1844.

Lucas, P.W., Hoare, M.G., Longmore, A., Schröder, A.C., Davis, C.J., Adamson, A., Bandyopadhyay, R.M., de Grijs, R., Smith, M., Gosling, A., Mitchison, S., Gáspár, A., Coe, M., Tamura, M., Parker, Q., Irwin, M., Hambly, N., Bryant, J., Collins, R.S., Cross, N., Evans, D.W., Gonzalez-Solares, E., Hodgkin, S., Lewis, J., Read, M., Riello, M., Sutorius, E.T.W., Lawrence, A., Drew, J.E., Dye, S., Thompson, M.A., 2008. The UKIDSS Galactic Plane Survey. Mon. Not. R. Astron. Soc. 391, 136–163. doi:10.1111/j.1365-2966.2008.13924.x, arXiv:0712.0100.

Lutovinov, A., Suleimanov, V., Manuel Luna, G.J., Sazonov, S., de Martino, D., Ducci, L., Doroshenko, V., Falanga, M., 2020. INTEGRAL View on cataclysmic variables and symbiotic binaries. New Astron. Rev. 91, 101547. doi:10.1016/j.newar.2020.101547, arXiv:2008.10665.

Masetti, N., Mason, E., Morelli, L., Cellone, S.A., McBride, V.A., Palazzi, E., Bassani, L., Bazzano, A., Bird, A.J., Charles, P.A., Dean, A.J., Galaz, G., Gehrels, N., Landi, R., Malizia, A., Minniti, D., Panessa, F., Romero, G.E., Stephen, J.B., Ubertini, P., Walter, R., 2008. Unveiling the nature of INTEGRAL objects through optical spectroscopy. VI. A multi-observatory identification campaign. Astron. & Astrophys. 482, 113–132. doi:10.1051/0004-6361:20079332, arXiv:0802.0988.

Masetti, N., Parisi, P., Jiménez-Bailón, E., Palazzi, E., Chavushyan, V., Bassani, L., Bazzano, A., Bird, A.J., Dean, A.J., Galaz, G., Landi, R., Malizia, A., Minniti, D., Morelli, L., Schiavone, F., Stephen, J.B., Ubertini, P., 2012. Unveiling the nature of INTEGRAL objects through optical spectroscopy. IX. Twenty two more identifications, and a glance into the far hard X-ray Universe. Astron. & Astrophys. 538, A123. doi:10.1051/0004-6361/201118559, arXiv:1201.1906.

Masetti, N., Parisi, P., Palazzi, E., Jiménez-Bailón, E., Chavushyan, V., Bassani, L., Bazzano, A., Bird, A.J., Dean, A.J., Charles, P.A., Galaz, G., Landi, R., Malizia, A., Mason, E., McBride, V.A., Minniti, D., Morelli, L., Schiavone, F., Stephen, J.B., Ubertini, P., 2010. Unveiling the nature of INTEGRAL objects through optical spectroscopy. VIII. Identification of 44 newly detected hard X-ray sources. Astron. & Astrophys. 519, A96. doi:10.1051/0004-6361/201014852, arXiv:1006.4513.

Masetti, N., Parisi, P., Palazzi, E., Jiménez-Bailón, E., Chavushyan, V., McBride, V., Rojas, A.F., Steward, L., Bassani, L., Bazzano, A., Bird, A.J., Charles, P.A., Galaz, G., Landi, R., Malizia, A., Mason, E., Minniti, D., Morelli, L., Schiavone, F., Stephen, J.B., Ubertini, P., 2013. Unveiling the nature of INTEGRAL objects through optical spectroscopy. X. A new multi-year, multi-observatory campaign. Astron. & Astrophys. 556, A120. doi:10.1051/0004-6361/201322026, arXiv:1307.2898.

Massaro, F., Marchesini, E.J., D'Abrusco, R., Masetti, N., Andruchow, I., Smith, H.A., 2017. Radio-weak BL Lac Objects in the Fermi Era. Astrophys. J. 834, 113. doi:10.3847/1538-4357/834/2/113, arXiv:1701.06067.

McConnell, D., Hale, C.L., Lenc, E., Banfield, J.K., Heald, G., Hotan, A.W., Leung, J.K., Moss, V.A., Murphy, T., O'Brien, A., Pritchard, J., Raja, W., Sadler, E.M., Stewart, A., Thomson, A.J.M., Whiting, M., Allison, J.R., Amy, S.W., Anderson, C., Ball, L., Bannister, K.W., Bell, M., Bock, D.C.J., Bolton, R., Bunton, J.D., Chippendale, A.P., Collier, J.D., Cooray, F.R., Cornwell, T.J., Diamond, P.J., Edwards, P.G., Gupta, N., Hayman, D.B., Heywood, I., Jackson, C.A., Koribalski, B.S., Lee-Waddell, K., McClure-Griffiths, N.M., Ng, A., Norris, R.P., Phillips, C., Reynolds, J.E., Roxby, D.N., Schinckel, A.E.T., Shields, M., Tremblay, C., Tzioumis, A., Voronkov, M.A., Westmeier, T., 2020. The Rapid ASKAP Continuum Survey I: Design and first results. Publ. Astron. Soc. Aust. 37, e048. doi:10.1017/pasa.2020.41, arXiv:2012.00747.

Mewe, R., Gronenschild, E.H.B.M., van den Oord, G.H.J., 1985. Calculated X-Radiation from Optically Thin Plasmas - Part Five. Astron. Astrophys. Suppl. 62, 197.

Minniti, D., Geisler, D., Alonso-García, J., Palma, T., Beamín, J.C., Borissova, J., Catelan, M., Clariá, J.J., Cohen, R.E., Contreras Ramos, R., Dias, B., Fernández-Trincado, J.G., Gómez, M., Hempel, M., Ivanov, V.D., Kurtev, R., Lucas, P.W., Moni-Bidin, C., Pullen, J., Ramírez Alegría, S., Saito, R.K., Valenti, E., 2017. New VVV Survey Globular Cluster Candidates in the Milky Way Bulge. Astrophys. J. Lett. 849, L24. doi:10.3847/2041-8213/aa95b8.

Molnar, T.A., Sanders, J.L., Smith, L.C., Belokurov, V., Lucas, P., Minniti, D., 2022. Variable star classification across the Galactic bulge and disc with the VISTA Variables in the Vía Láctea survey. Mon. Not. R. Astron. Soc. 509, 2566–2592. doi:10.1093/mnras/stab3116, arXiv:2110.15371.

Monet, D.G., Levine, S.E., Canzian, B., Ables, H.D., Bird, A.R., Dahn, C.C., Guetter, H.H., Harris, H.C., Henden, A.A., Leggett, S.K., Levison, H.F., Luginbuhl, C.B., Martini, J., Monet, A.K.B., Munn, J.A., Pier, J.R., Rhodes, A.R., Riepe, B., Sell, S., Stone, R.C., Vrba, F.J., Walker, R.L., Westerhout, G., Brucato, R.J., Reid, I.N., Schoening, W., Hartley, M., Read, M.A., Tritton, S.B., 2003. The USNO-B Catalog. Astron. J. 125, 984–993. doi:10.1086/345888, arXiv:astro-ph/0210694.

Mowlavi, N., Rimoldini, L., Evans, D.W., Riello, M., De Angeli, F., Palaversa, L., Audard, M., Eyer, L., Garcia-Lario, P., Gavras, P., Holl, B., Jevardat de Fombelle, G., Lecœur-Taïbi, I., Nienartowicz, K., 2021. Large-amplitude variables in Gaia Data Release 2. Multi-band variability characterization. Astron. & Astrophys. 648, A44. doi:10.1051/0004-6361/202039450, arXiv:2009.07746.

Oh, K., Koss, M., Markwardt, C.B., Schawinski, K., Baumgartner, W.H., Barthelmy, S.D., Cenko, S.B., Gehrels, N., Mushotzky, R., Petulante, A., Ricci, C., Lien, A., Trakhtenbrot, B., 2018. The 105-Month Swift-BAT All-sky Hard X-Ray Survey. Astrophys. J. Suppl. Ser. 235, 4. doi:10.3847/1538-4365/aaa7fd, arXiv:1801.01882.

Pojmanski, G., 2002. The All Sky Automated Survey. Catalog of Variable Stars. I. 0 h - 6 hQuarter of the Southern Hemisphere. Acta Astron. 52, 397–427. doi:10.48550/arXiv.astro-ph/0210283, arXiv:astro-ph/0210283.

Raymond, J.C., Smith, B.W., 1977. Soft X-ray spectrum of a hot plasma. Astrophys. J. Suppl. Ser. 35, 419–439. doi:10.1086/190486.

Reig, P., Milonaki, F., 2016. Accretion regimes in the X-ray pulsar 4U 1901+03. Astron. & Astrophys. 594, A45. doi:10.1051/0004-6361/201629200, arXiv:1608.06118.

Sasaki, R., Tsuboi, Y., Iwakiri, W., Nakahira, S., Maeda, Y., Gendreau, K., Corcoran, M.F., Hamaguchi, K., Arzoumanian, Z., Markwardt, C.B., Enoto, T., Sato, T., Kawai, H., Mihara, T., Shidatsu, M., Negoro, H., Serino, M., 2021. The RS CVn-type Star GT Mus Shows Most Energetic X-Ray Flares Throughout the 2010s. Astrophys. J. 910, 25. doi:10.3847/1538-4357/abde38, arXiv:2103.16822.

Saxton, R.D., Read, A.M., Esquej, P., Freyberg, M.J., Altieri, B., Bermejo, D., 2008. The first XMM-Newton slew survey catalogue: XMMSL1. Astron. & Astrophys. 480, 611–622. doi:10.1051/0004-6361:20079193, arXiv:0801.3732.

Saydjari, A.K., Schlafly, E.F., Lang, D., Meisner, A.M., Green, G.M., Zucker, C., Zelko, I., Speagle, J.S., Daylan, T., Lee, A., Valdes, F., Schlegel, D., Finkbeiner, D.P., 2023. The Dark Energy Camera Plane Survey 2 (DECaPS2): More Sky, Less Bias, and Better Uncertainties. Astrophys. J. Suppl. Ser. 264, 28. doi:10.3847/1538-4365/aca594, arXiv:2206.11909.

Secrest, N.J., Dudik, R.P., Dorland, B.N., Zacharias, N., Makarov, V., Fey, A., Frouard, J., Finch, C., 2015. Identification of 1.4 Million Active Galactic Nuclei in the Mid-Infrared using WISE Data. Astrophys. J. Suppl. Ser. 221, 12. doi:10.1088/0067-0049/221/1/12, arXiv:1509.07289.

Sguera, V., Bazzano, A., Fiocchi, M., Ubertini, P., Natalucci, L., Sidoli, L., Bird, A.J., Kuulkers, E., Bassani, L., 2016. INTEGRAL detection of bright hard X-ray emission from the RS CVn star GT Mus. The Astronomer's Telegram 9255, 1.

Skrutskie, M.F., Cutri, R.M., Stiening, R., Weinberg, M.D., Schneider, S., Carpenter, J.M., Beichman, C., Capps, R., Chester, T., Elias, J., Huchra, J., Liebert, J., Lonsdale, C., Monet, D.G., Price, S., Seitzer, P., Jarrett, T., Kirkpatrick, J.D., Gizis, J.E., Howard, E., Evans, T., Fowler, J., Fullmer, L., Hurt, R., Light, R., Kopan, E.L., Marsh, K.A., McCallon, H.L., Tam, R., Van Dyk, S., Wheelock, S., 2006. The Two Micron All Sky Survey (2MASS). Astron. J. 131, 1163–1183. doi:10.1086/498708.

Smith, L.C., Lucas, P.W., Kurtev, R., Smart, R., Minniti, D., Borissova, J., Jones, H.R.A., Zhang, Z.H., Marocco, F., Contreras Peña, C., Gromadzki, M., Kuhn, M.A., Drew, J.E., Pinfield, D.J., Bedin, L.R., 2018. VIRAC: the VVV Infrared Astrometric Catalogue. Mon. Not. R. Astron. Soc. 474, 1826–1849. doi:10.1093/mnras/stx2789, arXiv:1710.08919.

Stephen, J.B., Bassani, L., Malizia, A., Bazzano, A., Ubertini, P., Bird, A.J., Dean, A.J., Lebrun, F., Walter, R., 2006. Using the ROSAT catalogues to find counterparts for the second IBIS/ISGRI survey sources. Astron. & Astrophys. 445, 869–873. doi:10.1051/0004-6361:20053958, arXiv:astro-ph/0509620.

Stocke, J.T., Morris, S.L., Gioia, I.M., Maccacaro, T., Schild, R., Wolter, A., Fleming, T.A., Henry, J.P., 1991. The Einstein Observatory Extended Medium-Sensitivity Survey. II. The Optical Identifications. Astrophys. J. Suppl. Ser. 76, 813. doi:10.1086/191582.

Suleimanov, V.F., Doroshenko, V., Werner, K., 2022. Hard X-ray luminosity functions of cataclysmic variables: joint Swift/BAT and Gaia data. Mon. Not. R. Astron. Soc. 511, 4937–4945. doi:10.1093/mnras/stac417, arXiv:2202.05809.

Tomsick, J.A., Bodaghee, A., Chaty, S., Rodriguez, J., Rahoui, F., Halpern, J., Kalemci, E., Özbey Arabaci, M., 2012. Localizing INTEGRAL Sources with Chandra: X-Ray and Multiwavelength Identifications and Energy Spectra. Astrophys. J. 754, 145. doi:10.1088/0004-637X/754/2/145, arXiv:1206.1071.

Turner, M.J.L., Reeves, J.N., Ponman, T.J., Arnaud, M., Barbera, M., Bennie, P.J., Boer, M., Briel, U., Butler, I., Clavel, J., Dhez, P., Cordova, F., Dos Santos, S., Ferrando, P., Ghizzardi, S., Goodall, C.V., Griffiths, R.G., Hochedez, J.F., Holland, A.D., Jansen, F., Kendziorra, E., Lagostina, A., Laine, R., La Palombara, N., Lortholary, M., Mason, K.O., Molendi, S., Pigot, C., Priedhorsky, W., Reppin, C., Rothenflug, R., Salvetat, P., Sauvageot, J., Schmitt, D., Sembay, S., Short, A., Strüder, L., Trifoglio, M., Trümper, J., Vercellone, S., Vigroux, L., Villa, G., Ward, M., 2001. XMM-Newton first-light observations of the Hickson galaxy group 16. Astron. & Astrophys. 365, L110–L115. doi:10.1051/0004-6361:20000070, arXiv:astro-ph/0010612.

Ubertini, P., Lebrun, F., Di Cocco, G., Bazzano, A., Bird, A.J., Broenstad, K., Goldwurm, A., La Rosa, G., Labanti, C., Laurent, P., Mirabel, I.F., Quadrini, E.M., Ramsey, B., Reglero, V., Sabau, L., Sacco, B., Staubert, R., Vigroux, L., Weisskopf, M.C., Zdziarski, A.A., 2003. IBIS: The Imager on-board INTEGRAL. Astron. & Astrophys. 411, L131–L139. doi:10.1051/0004-6361:20031224.

Webb, N.A., Coriat, M., Traulsen, I., Ballet, J., Motch, C., Carrera, F.J., Koliopanos, F., Authier, J., de la Calle, I., Ceballos, M.T., Colomo, E., Chuard, D., Freyberg, M., Garcia, T., Kolehmainen, M., Lamer, G., Lin, D., Maggi, P., Michel, L., Page, C.G., Page, M.J., Perea-Calderon, J.V., Pineau, F.X., Rodriguez, P., Rosen, S.R., Santos Lleo, M., Saxton, R.D., Schwope, A., Tomás, L., Watson, M.G., Zakardjian, A., 2020. The XMM-Newton serendipitous survey. IX. The fourth XMM-Newton serendipitous source catalogue. Astron. & Astrophys. 641, A136. doi:10.1051/0004-6361/201937353, arXiv:2007.02899.

White, R.L., Becker, R.H., Helfand, D.J., 2005. New Catalogs of Compact Radio Sources in the Galactic Plane. Astron. J. 130, 586–596. doi:10.1086/431249, arXiv:astro-ph/0501607.

Wright, E.L., Eisenhardt, P.R.M., Mainzer, A.K., Ressler, M.E., Cutri, R.M., Jarrett, T., Kirkpatrick, J.D., Padgett, D., McMillan, R.S., Skrutskie, M., Stanford, S.A., Cohen, M., Walker, R.G., Mather, J.C., Leisawitz, D., Gautier, Thomas N., I., McLean, I., Benford, D., Lonsdale, C.J., Blain, A., Mendez, B., Irace, W.R., Duval, V., Liu, F., Royer, D., Heinrichsen, I., Howard,

J., Shannon, M., Kendall, M., Walsh, A.L., Larsen, M., Cardon, J.G., Schick, S., Schwalm, M., Abid, M., Fabinsky, B., Naes, L., Tsai, C.W., 2010. The Wide-field Infrared Survey Explorer (WISE): Mission Description and Initial On-orbit Performance. Astron. J. 140, 1868–1881. doi:10.1088/0004-6256/140/6/1868, arXiv:1008.0031.